The Astrophysical Journal, 947:27 (18pp), 2023 April 10 https://doi.org/10.3847/1538-4357/acb690

Strong Variability in AzV 493, an Extreme Oe-type Star in the SMC

M. S. Oey[1], N. Castro[2], M. Renzo[3], I. Vargas-Salazar[1], M. W. Suffak[4], M. Ratajczak[5], J. D. Monnier[1], M. K. Szymanski[5], G. D. Phillips[1], N. Calvet[1], A. Chiti[6,7], G. Micheva[1,8], K. C. Rasmussen[1,9], and R. H. D. Townsend[10]
[1] Astronomy Department, University of Michigan, 1085 South University Avenue, Ann Arbor, MI 48109, USA; msoey@umich.edu
[2] Leibniz-Institut für Astrophysik Potsdam (AIP), An der Sternwarte 16, D-14482, Potsdam, Germany
[3] Center for Computational Astrophysics, Flatiron Institute, 162 5th Avenue, New York, NY 10010, USA
[4] Department of Physics and Astronomy, Western University, London, ON N6A 3K7, Canada
[5] Astronomical Observatory, University of Warsaw, Al. Ujazdowskie 4, 00-478 Warszawa, Poland
[6] Department of Astronomy & Astrophysics, University of Chicago, 5640 South Ellis Avenue, Chicago, IL 60637, USA
[7] Kavli Institute for Cosmological Physics, University of Chicago, Chicago, IL 60637, USA
[8] Present address: Leibniz-Institut für Astrophysik Potsdam (AIP), An der Sternwarte 16, D-14482, Potsdam, Germany
[9] Present address: Astronomy Department, University of Washington, Box 351580, Seattle, WA 98195, USA
[10] Astronomy Department, University of Wisconsin, Madison, WI 53706, USA
Received 2022 July 5; revised 2023 January 23; accepted 2023 January 23; published 2023 April 14

Abstract

We present 18 yr of OGLE photometry together with spectra obtained over 12 yr revealing that the early Oe star AzV 493 shows strong photometric ($\Delta I < 1.2$ mag) and spectroscopic variability with a dominant, 14.6 yr pattern and ~40 day oscillations. We estimate the stellar parameters $T_{\rm eff} = 42{,}000$ K, $\log L/L_\odot = 5.83 \pm 0.15$, $M/M_\odot = 50 \pm 9$, and $v \sin i = 370 \pm 40$ km s^{-1}. Direct spectroscopic evidence shows episodes of both gas ejection and infall. There is no X-ray detection, and it is likely a runaway star. The star AzV 493 may have an unseen companion on a highly eccentric ($e > 0.93$) orbit. We propose that close interaction at periastron excites ejection of the decretion disk, whose variable emission-line spectrum suggests separate inner and outer components, with an optically thick outer component obscuring both the stellar photosphere and the emission-line spectrum of the inner disk at early phases in the photometric cycle. It is plausible that AzV 493's mass and rotation have been enhanced by binary interaction followed by the core-collapse supernova explosion of the companion, which now could be either a black hole or a neutron star. This system in the Small Magellanic Cloud can potentially shed light on OBe decretion disk formation and evolution, massive binary evolution, and compact binary progenitors.

Unified Astronomy Thesaurus concepts: Early-type stars (430); Oe stars (1153); Be stars (142); Circumstellar disks (235); Interacting binary stars (801); Compact objects (288); Runaway stars (1417)

1. Introduction

Binary interactions are now understood to be a fundamental component of massive star evolution, and they are the progenitors of a wide variety of energetic phenomena, including high-mass X-ray binaries (HMXBs), ultraluminous X-ray sources, stripped-envelope core-collapse supernovae (SNe), and gravitational-wave events. A consensus is emerging that classical OBe stars appear to originate from close massive binary systems, wherein they have spun up through mass and angular momentum transfer from their mass donors (e.g., Pols et al. 1991; Bodensteiner et al. 2020; Vinciguerra et al. 2020; see also Rivinius et al. 2013 for a review). When donor stars subsequently explode as SNe, the resulting postexplosion bound binaries are more likely to be eccentric, since they result from tight binaries (e.g., Brandt & Podsiadlowski 1995; Tauris & Takens 1998; Renzo et al. 2019). Thus, a substantial subset of classical OBe stars are likely to have eccentric orbits. In this paper, we present photometric and spectroscopic time-series data showing that the star AzV 493 exhibits dramatic variability and may be an eccentric binary system.

Object AzV 493 (Azzopardi et al. 1975), or [M2002]SMC-77616 (Massey 2002), was identified as an extreme classical Oe star by Golden-Marx et al. (2016). In that work, it was found to be the earliest classical Oe star in our sample of field OB stars in the Small Magellanic Cloud (SMC) based on a spectrum obtained in 2009 that shows double-peaked emission not only in the Balmer lines but also in He I and He II λ4686, the latter feature being rarely observed in other Oe stars (Conti & Leep 1974). Specifically, it is classified as an Ope star, indicating that the He I absorption lines show infilled emission (Sota et al. 2011).

As an extreme object, AzV 493 offers unique opportunities to study massive binary evolution and decretion disk formation, structure, and dynamics. Section 2 presents the unusual light curve and periodicity, and Section 3 presents our multi-epoch spectroscopy with the resulting derived stellar parameters and individual spectral features. We then present two possible models for the AzV 493 system in Sections 4 and 5, one based on ejection of an optically thick disk near periastron and the other based on disk growth and disruption. Section 6 discusses the likely binary origin of the system, and Section 7 summarizes our findings.

2. Photometric Light Curve

2.1. Long-term Light Curve

The *I*- and *V*-band light curves of AzV 493 from the Optical Gravitational Lensing Experiment (OGLE) project (Udalski et al. 2008, 2015) are presented in Figure 1. The *I* band shows a

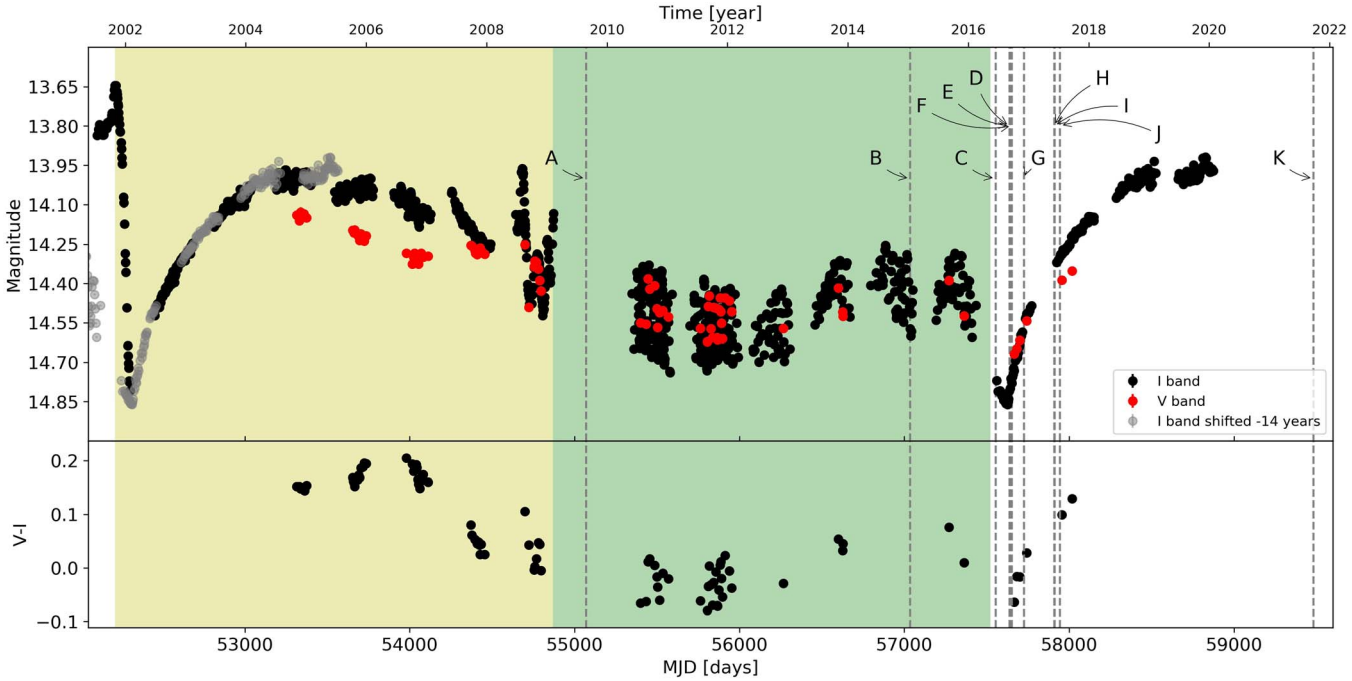

Figure 1. The AzV 493 OGLE light curves in the *I* (black) and *V* (red) bands. The last segment of the *I*-band curve is overplotted (gray dots) on the beginning of the data set phase 14.55 yr (5311 days) earlier. The $V-I$ is shown in the lower panel. The dashed lines mark the epochs for the observed spectra, assigned alphabetically in chronological sequence. The green shaded regions show consecutive 2656 day segments starting with the light-curve maximum in 2001.

short eruption with the peak of the light curve on MJD 52,212, followed by an abrupt decline of approximately 1.2 mag to a minimum on MJD 52,303 in early 2002. After this, the star eventually recovers its original luminosity. Another photometric minimum is seen in 2016 on MJD 57,626, followed by the same brightening pattern. The gray symbols in Figure 1 show the *I*-band photometry from the 2016 cycle overplotted on the data from the 2002 cycle. This shows that the minimum luminosity and subsequent increase are quantitatively identical, although the photometry immediately preceding the minimum differs. Cross-correlating these segments yields a long-cycle period of 5311 days (14.55 yr). There is no evidence of a similar eruption preceding the minimum in the 2016 cycle on the same 91 day timescale, although the photometry is incomplete in this range.

After the minimum, the brightness increases and then starts to gradually decrease again over a period of several years. In approximately 2008, AzV 493 appears to go into a multiple-outburst event. After this, the light curve drastically changes, showing a multimode pulsation behavior that evolves with time (Section 2.2). The pulsation ends with another 0.2–0.3 mag drop followed by a steady increase, repeating the light-curve cycle that started in 2002, 14.55 yr before.

2.2. Photometric Oscillations

Figure 2 shows short-term variability on the order of 30–45 days. We quantify the evolution of these oscillations seen in the *I*-band light curve using generalized Lomb–Scargle periodograms (Zechmeister & Kürster 2009) for the six contiguous OGLE data sets from 2010 to 2016 (Figure 1). The individual fits to these six ranges are shown in the Appendix. Comparison of the periods shown in Figure 3 with the light curve (Figure 1) shows that they qualitatively appear to correlate with stellar brightness.

The OGLE survey provides *V*-band magnitudes for a subset of the survey epochs, which are shown in red in Figure 1. Figure 4 displays the color–magnitude diagram (CMD) in *V* versus $V-I$ for those days where both bands were observed. Figure 4 (left panel) compares AzV 493's color variations with data for the remainder of the RIOTS4 sample stars (Lamb et al. 2016). The latter correspond to single-epoch photometry from the OGLE catalog of Poleski et al. 2012. Those stars classified as OBe stars by Lamb et al. (2016) are marked in the figure. The blue plume of non-emission-line stars is clearly separated from the cloud of OBe stars at redder colors in the CMD, a phenomenon already known from different photometric bands (e.g., Bonanos et al. 2010; Castro et al. 2018). The color variation of AzV 493 spans almost the entire range of $V-I$ colors covered by the emission-line stars.

Figure 4 (right panel) shows a zoom in the CMD with the path of AzV 493 traced out. The star appears red during the broad peak of the light curve around 2006 (Figure 1) and then moves to bluer colors, reaching the bluest $V-I$ color during the pulsation phase. In approximately 2017, when the light curve is brightening after the minimum, AzV 493 shows redder colors again, moving to the original position observed in 2005 with $V-I\sim 0.18$.

Similar, semiperiodic variability with timescales on the order of weeks to months is seen in many other OBe stars, and their origin is unknown (e.g., Labadie-Bartz et al. 2017). Proposed explanations include forms of nonradial pulsation of the star and transitory or orbiting density enhancements in the disk, which may be the most likely scenario. The associated cyclical variation in the CMD (Figure 4) is also consistent with some kind of stellar radial pulsation. This is supported by the correlation between period and luminosity (see Figures 3 and 4). In that case, the relatively long period implies that they could be an induced gravity mode or pulsational instability. However, there are many other possible explanations, perhaps including interactions with another star in a close orbit. We note that de Wit et al. (2006; see also Rivinius et al. 2013) reported similar loop-like excursions in the CMD of other OBe stars and ascribed the counterclockwise variation to the

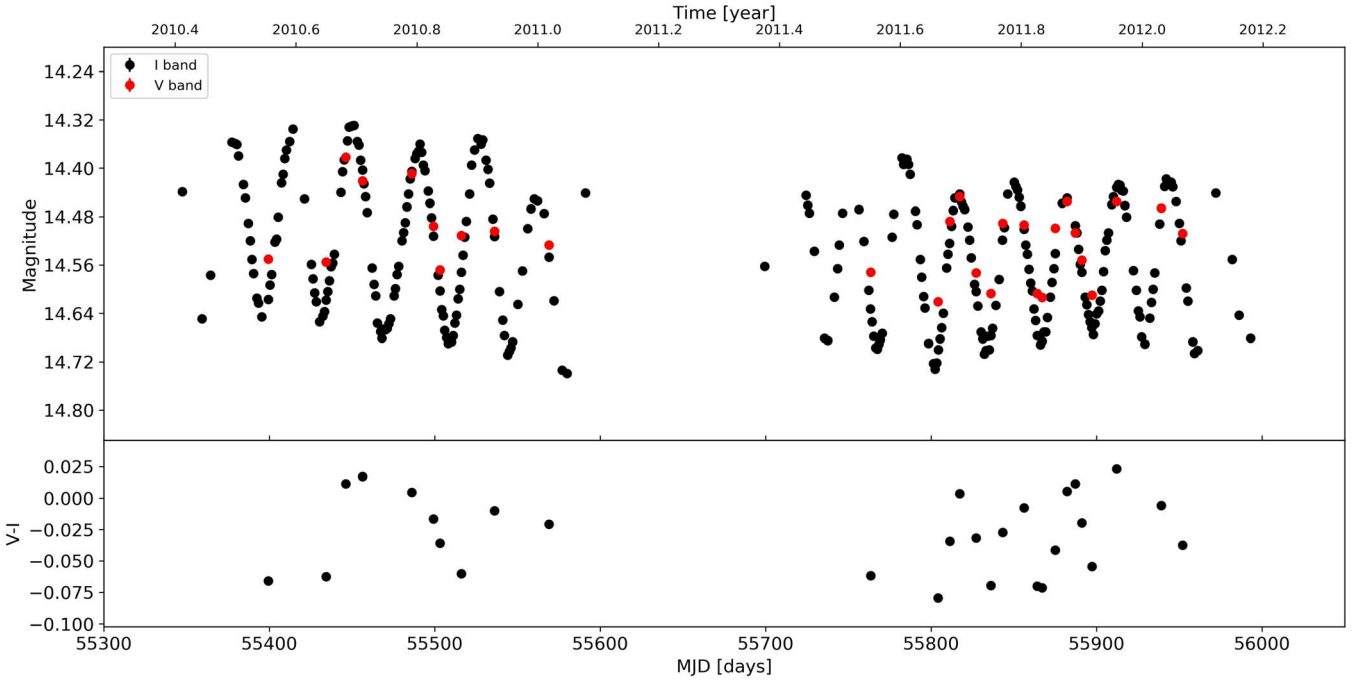

Figure 2. Zoom on light curve (top) showing ∼40 day oscillations and color variation (bottom).

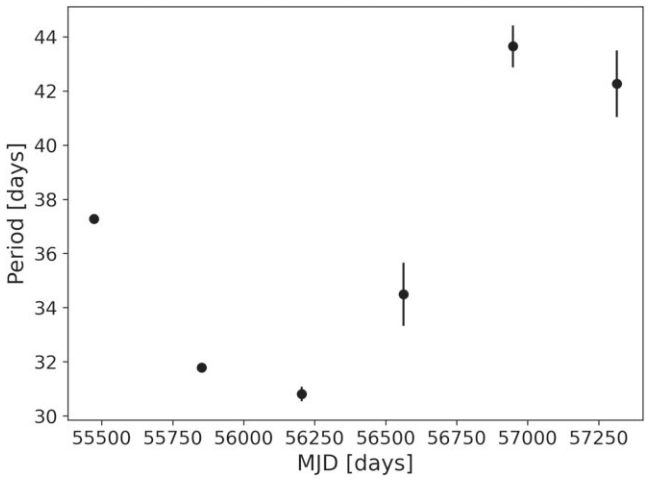

Figure 3. Fitted periods for the six contiguous OGLE data sets between ∼2010 and 2016 as a function of time.

formation and dissipation of the circumstellar decretion disks in those objects.

2.3. Light-curve Period

It is possible that the multiple-outburst event in 2008–2009 may represent another periastron. Figure 1 shows the 5311 day cycle initiated at the light-curve peak at MJD 52,212 instead of at the minima. We see that the mid-cycle occurs during this multiple-outburst event, although due to the OGLE observing cadence, it is unclear whether it occurs near the end or middle. In Section 3 below, we show that the spectrum obtained around this time, epoch A (Figure 1), shows an unusually strong emission-line spectrum, consistent with maximum disk activation and flaring. However, the light curve does not repeat the cycle minimum seen in 2002 and 2016, and OBe stars are known to show temporary outbursts of activity (e.g., Labadie-Bartz et al. 2017; Baade et al. 2018).

Thus, it is not clear whether 2008–2009 corresponds to the mid-cycle or not. The light curve does not repeat regularly in detail, and we caution that the period, if the system is a binary, is uncertain. Assuming that there is indeed a fundamental physical period, the same phases may not all generate the same observational signatures, which may depend on other factors such as disk orientation and/or varying physical processes. In what follows, we adopt a system period of 5311 (2656) days, or 14.55 (7.28) yr, where the values in parentheses allow for the possibility that the period may be half of the long cycle.

3. Spectroscopy

Spectroscopic observations of AzV 493 were obtained in the course of the RIOTS4 spectroscopic survey of field OB stars in the SMC (Lamb et al. 2016) and follow-up radial velocity (RV) monitoring of the SMC Wing region (Vargas-Salazar et al. 2023, in preparation). The observations were carried out using the Magellan telescopes at Las Campanas, Chile. Three different spectrographs were used: IMACS (Bigelow & Dressler 2003), MIKE (Bernstein et al. 2003), and M2FS (Mateo et al. 2012). Table 1 gives the details of our spectroscopic observations, including the Modified Julian Date (MJD), signal-to-noise ratio (S/N), spectral resolution, spectral range, phase in the light-curve cycle, RV, Hβ peak separation (Section 3.2), and instrument used. Figure 5 displays the 11 spectra in chronological sequence, labeled A–K as shown.

The IMACS was operated by default in multislit mode with the f/4 camera and 1200 lines mm^{-1} grating, which provides a resolving power of $R \sim 3000$ and wavelength coverage spanning ∼3800–5200 Å. One observation (epoch I) was observed with the f/2 camera, resulting in lower resolution (Table 1). The reduction was performed using the COSMOS pipeline.[11] MIKE data were obtained using a 1″ slit width for a spectral resolution of $R \sim 28{,}000$, covering the wavelength

[11] http://code.obs.carnegiescience.edu/cosmos

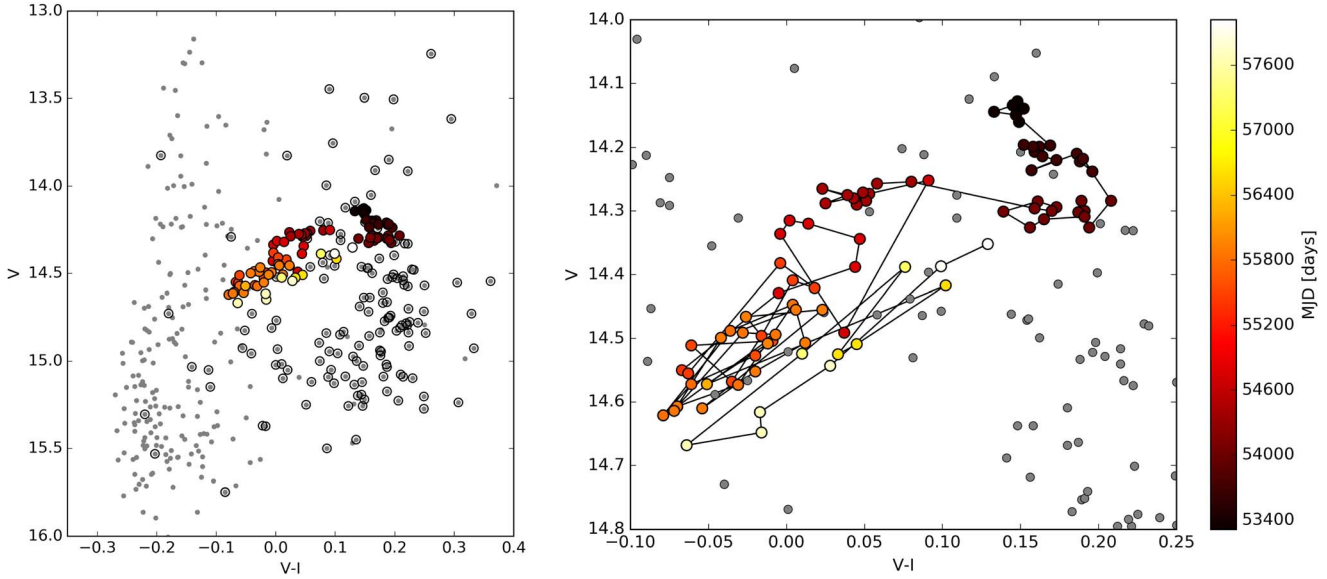

Figure 4. The CMD based on available *V*- and *I*-band OGLE photometry (see Figure 1). The variation of AzV 493 in the CMD is colored according to the MJD and compared to single-epoch OGLE photometry (Poleski et al. 2012) for the RIOTS4 OB star sample (Lamb et al. 2016; gray dots). Objects classified as OBe by Lamb et al. (2016) are highlighted with circles. The right panel is a zoom of the same data around the track of AzV 493.

Table 1
Spectroscopic Observations of AzV 493

Epoch	Date (UTC)	MJD	S/N	*R*	Wavelength Range (Å)	Phase[a]	RV (km s^{-1})	Δv(Hβ)[b] (km s^{-1})	Instrument
A	2009-8-26T01:43:36.0	55,069.071944	140	3000	3825–5422	0.538 (0.076)	152 ± 200	279	IMACS
B	2015-1-14T02:12:03.0	57,036.091701	120	28,000	3362–9397	0.908 (0.817)	192 ± 18	(213)[c]	MIKE
C	2016-6-15T07:47:54.3	57,554.324935	130	3000	3879–5479	0.006 (0.012)	171 ± 60	346	IMACS
D	2016-9-8T01:42:08.0	57,639.070926	60	28,000	4079–4466	0.022 (0.044)	217 ± 50	⋯	M2FS
E	2016-9-11T02:49:33.0	57,642.117743	90	28,000	4080–4465	0.022 (0.045)	239 ± 46	⋯	M2FS
F	2016-9-22T05:36:51.0	57,653.233924	150	28,000	3538–9397	0.024 (0.049)	192 ± 29	334	MIKE
G	2016-12-4T04:09:41.5	57,726.173397	110	3000	3862–5458	0.038 (0.076)	243 ± 38	319	IMACS
H	2017-6-5T06:35:11.2	57,909.274435	50	3000	3871–5471	0.073 (0.145)	235 ± 54	322	IMACS
I	2017-6-7T08:08:18.9	57,911.339108	130	1300	3900–8000	0.073 (0.146)	231 ± 83	295	IMACS[d]
J	2017-7-10T09:05:00.5	57,944.378478	190	3000	3854–5468	0.079 (0.159)	181 ± 39	303	IMACS
K	2021-9-25T07:38:18.0	59,482.318264	210	28,000	3362–9397	0.369 (0.738)	183 ± 17	289	MIKE

Notes.
[a] Phase relative to the light-curve peak at MJD 52,212 (54,868), adopting a period of 5311 (2655.5) days.
[b] Hβ peak separation obtained by fitting two Gaussians with a fixed width of 2 Å (∼120 km s^{-1}).
[c] Epoch B does not show a double-peaked profile (see Figure 7 and Section 3.4); the value for Δv(Hβ) assumes that two components exist, as they do for other epochs.
[d] Epoch I was observed with the f/2 camera, while the other IMACS observations were obtained with the f/4 camera.

range ∼3600–10000 Å. The spectra were processed with the the Carnegie Python (CARPY[12]) pipeline software (Kelson et al. 2000; Kelson 2003), except for epoch B, which was extracted using IRAF.[13] The M2FS data were observed using a custom filter yielding ∼4080–4470 Å wavelength coverage at $R \sim 28{,}000$. The data were processed following the standard steps in fiber spectroscopic reduction using IRAF/PyRAF tasks implemented within Python and designed for this instrument (see Walker et al. 2015).

Figure 5 shows strong variability in the spectrum of AzV 493. The weaker epochs show a typical OBe spectrum, with only Hβ showing double-peaked emission and Hγ and Hδ absorption features showing evidence of infill, whereas epochs A, B, and K show stronger emission-line spectra, with Hγ and He I often in emission. Epoch F shows strong, high-order Balmer emission and inverse P Cygni features. These epochs will be discussed in Sections 3.3 and 3.4.

3.1. Stellar Fundamental Parameters

The photospheric He II λ4200, λ4541, and λ5411 lines at all epochs confirm the early O spectral type assigned by Golden-Marx et al. (2016). To improve the S/N in the He II λ4541 absorption line, we combine epochs C, G, H, and J, which are all IMACS spectra obtained in 2016–2017. We use this composite spectrum to estimate the projected rotational velocity ($\upsilon \sin i$) using the IACOB-BROAD code (Simón-Díaz & Herrero 2014, 2007). We obtain $\upsilon \sin i = 370 \pm 40$

[12] http://code.obs.carnegiescience.edu/mike
[13] IRAF was distributed by the National Optical Astronomy Observatory, which was managed by the Association of Universities for Research in Astronomy (AURA) under a cooperative agreement with the National Science Foundation.

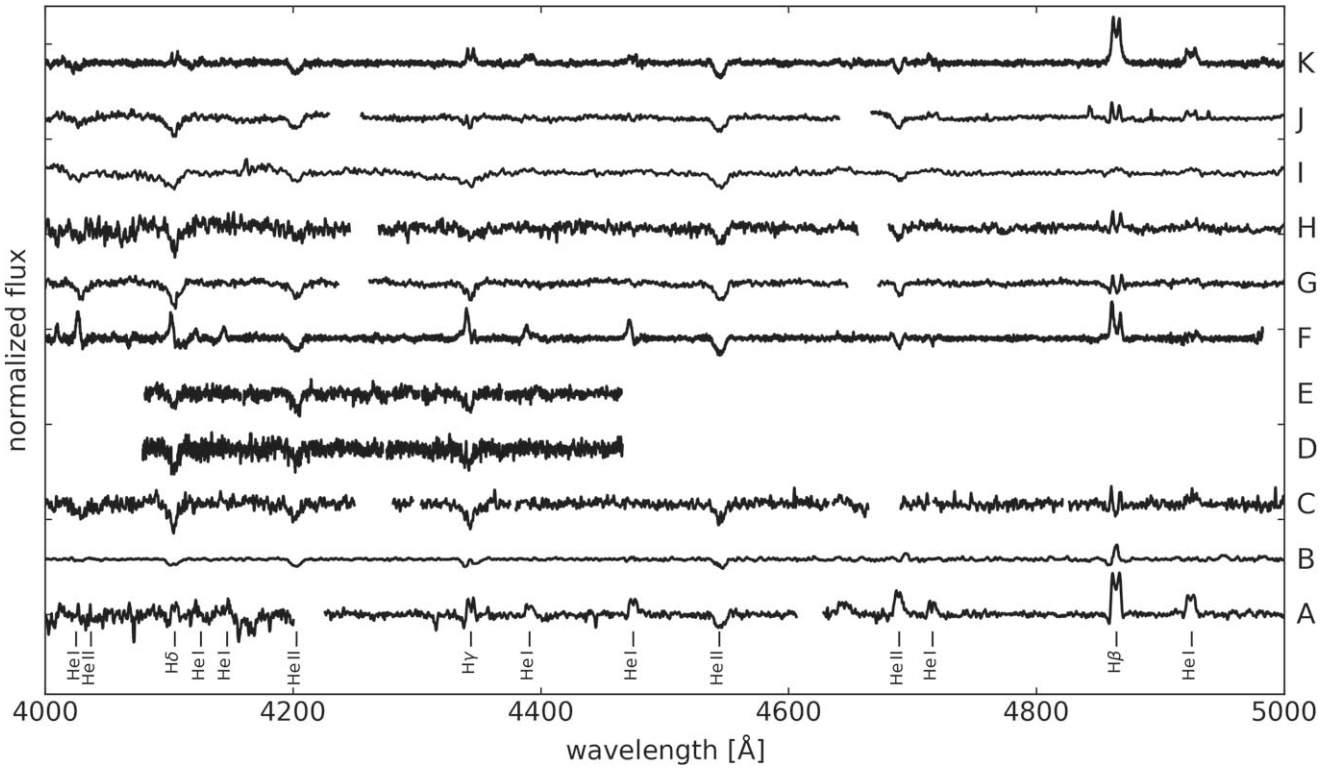

Figure 5. The AzV 493 multi-epoch spectroscopic observations sorted by MJD and normalized to the continuum. Epoch I is low resolution (Table 1).

km s^{-1}. As discussed in Section 4, the angle of inclination i is likely high based on the amount of obscuration from the disk, thus the rotational velocity might be $\lesssim$450 km s^{-1}.

The combined spectrum was modeled using the stellar atmosphere code FASTWIND (Santolaya-Rey et al. 1997; Puls et al. 2005; Rivero González et al. 2012) using the same technique and stellar grid described in Castro et al. (2018). The cores of the Balmer lines are omitted from the fit to ameliorate contamination from disk emission. Our best model yields an effective temperature $T_{\rm eff} = 42{,}000$ K and surface gravity $\log g = 3.4$ dex, which reproduce the main He I and He II lines (Figure 6). Since He I photospheric features are not detected, this $T_{\rm eff}$ may be a lower limit. The derived temperature is consistent with an O3–5 spectral type (Martins & Palacios 2021), matching the early O-type classification of AzV 493 (Lamb et al. 2016). However, we caution that the wings of the Balmer lines, which are the main spectroscopic anchors for deriving the surface gravity, may be affected by the circumstellar emission, resulting in an underestimate of $\log g$, as found for OBe stars by Castro et al. (2018).

The stellar luminosity was calculated using the optical and IR photometry for AzV 493 (Massey 2002; Skrutskie et al. 2006), adopting a distance to the SMC of 62.1 kpc (Graczyk et al. 2014) and the synthetic FASTWIND spectral energy distribution (SED) derived above. We explored the extinction curves published by Fitzpatrick & Massa (2007) until the observed photometry was reproduced by the FASTWIND synthetic SED. We obtain a luminosity $\log L/L_\odot = 5.83 \pm 0.15$ and radius $R_\star/R_\odot = 15 \pm 3$, in agreement with the expected values for an early O-type star of luminosity class III—V (e.g., Martins et al. 2005). We compare the position of AzV 493 in the Hertzsprung–Russell diagram with the rotating evolutionary tracks by Brott et al. (2011) for SMC metallicity. Based on the $T_{\rm eff}$ and $L/L_\odot$ and their respective uncertainties, we estimate that the stellar mass is $M/M_\odot = 50 \pm 9$. If the observed luminosity is overestimated by the inferred $\log g$ or includes a contribution from a non–compact binary companion and/or the disk continuum, then the stellar mass may be somewhat overestimated; for reference, a factor of 2 overestimate in luminosity implies $M/M_\odot \sim 40$.

3.2. Hβ Emission-line Profile

Variability in the emission lines is a common characteristic of the Be phenomenon (e.g., Rivinius et al. 2013; Richardson et al. 2021). One effect is the violet-to-red (V/R) variations, which are cycles that can last weeks or decades. The V/R variations describe changes in the dominant peak strength for the double-peaked emission lines observed in some stars. These cycles are attributed to variation in the morphology and density of the circumstellar disks (Poeckert 1982; Okazaki 1991).

Figure 7 shows Hβ profiles in the spectroscopic epochs where this line is available and Gaussian models are used to disentangle the V and R components. The two peaks are clearly resolved in all of our observations of Hβ, except for epoch B, which instead shows a P Cygni profile (Figures 5 and 7; see Section 3.4). Table 1 gives the peak separations ΔHβ fitted in Figure 7. The V peak is usually more prominent than R. There may be a long-timescale V/R cycle, but further spectroscopic monitoring is needed to determine whether V/R indeed oscillates or the existence of any trend in ΔHβ with phase.

3.3. Epochs A and K: Evidence of Disk Evolution

Epoch A is observed at a phase of 0.54 (0.08), soon after the apparent eruption event in 2009 (Figure 1, Table 1). This spectrum shows the strongest helium line emission (Figure 5), although we have no other spectroscopic observations within several years of this data point. Only photospheric He II is seen

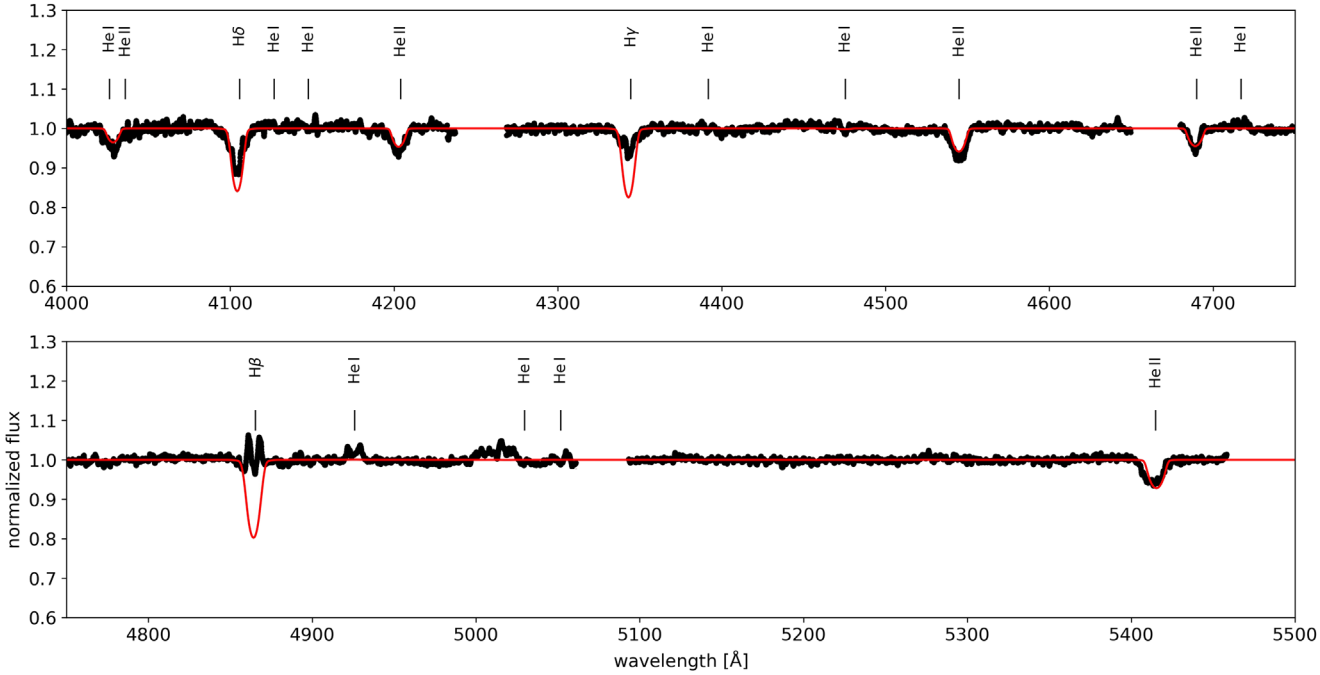

Figure 6. Spectroscopic analysis of the composite IMACS spectrum from epochs C, G, H, and J (black; see Figure 5). The best FASTWIND (Santolaya-Rey et al. 1997; Puls et al. 2005; Rivero González et al. 2012) stellar atmosphere synthetic model is overplotted (red). The main transitions used in the analysis are marked.

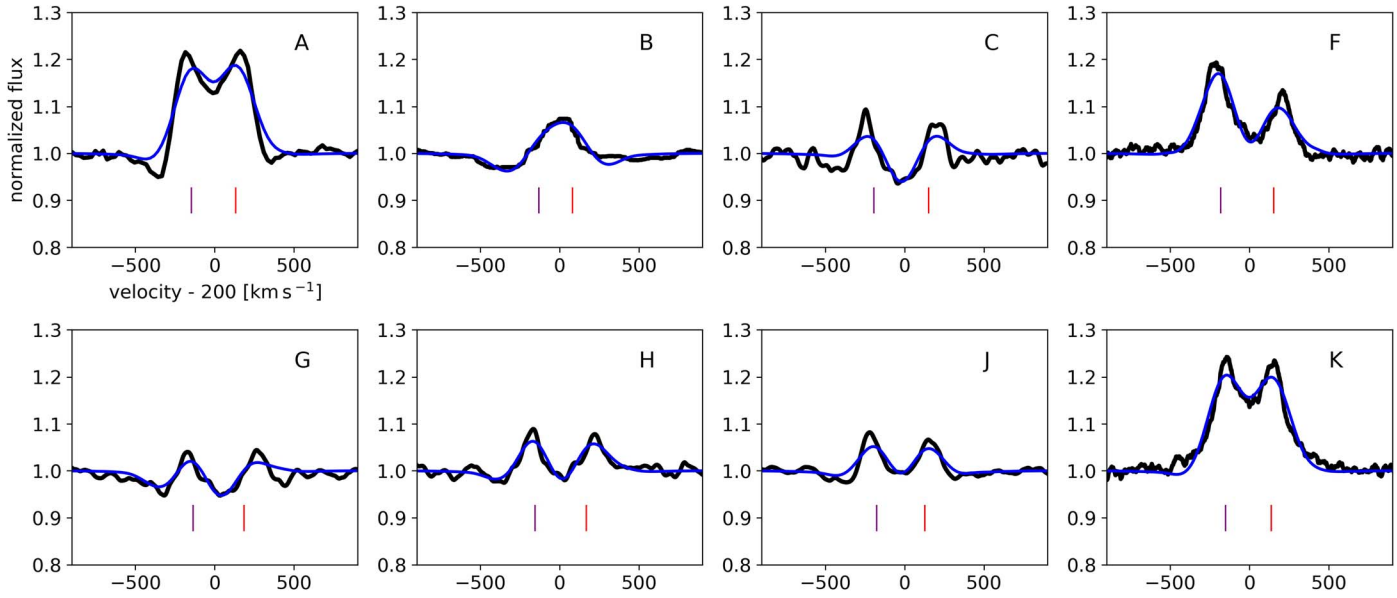

Figure 7. The Hβ emission-line profiles from our spectra of AzV 493. The best-fit photospheric model (Figure 6) is subtracted, after which the V and R components are fitted by two Gaussian profiles having fixed widths of 2 Å. The figure shows the data overplotted by these summed fitted Gaussians. The resulting peak values are shown by the vertical lines, and their separations are given in Table 1. Epoch I has low spectral resolution and is not included in this figure.

in absorption in this spectrum; the H I and He I lines are all in emission or filled in. Moreover, He II λ4686 is also in emission, which prompted Golden-Marx et al. (2016) to identify this spectrum as the hottest known observation of the OBe phenomenon. Nebular He II is only generated by the very hottest O stars (e.g., Martins & Palacios 2021).

All of the emission lines in epoch A are double-peaked. The Hβ and Hγ show larger peak separations than the He I and He II emission lines. For a Keplerian disk, this would imply that the higher-temperature species is dominated by larger radii than the Hβ and Hγ emission. Figure 5 shows that the emission is slightly redshifted relative to the photospheric Balmer absorption.

Epoch K, observed at phase 0.37 (0.74; Figure 5, Table 1), shows the opposite relation between ionization and disk radius. Here the He I lines have larger peak separations than Hβ, implying that the hotter species dominates at smaller radii, unlike epoch A. We also see that the Hβ and Hγ line profiles show high-velocity wings that are not observed at other epochs, consistent with high-velocity gas at smaller orbital radii. Epoch K is similar in emission-line strength to epoch A and

shows He I in emission, but He II λ4686 is in absorption in this observation, as it is in all other observations of this line.

3.4. Epochs B and F: Gas Outflow and Infall

Epoch B shows P Cygni emission-line profiles in Hβ and Hγ (Figure 5 and 7), suggesting an outflow episode. This is also the only spectrum obtained during the period where the strong pulsations dominate the flux (Figure 1), and it is observed at the latest phase, 0.91 (0.82). Figure 13 shows that the observation coincides with a local minimum in the light curve. Thus, the P Cygni features could suggest that the pulsations may be directly linked to mass ejection, since it coincides with the star reaching its smallest radius.

The spectrum of epoch F is dramatically different from most of the other spectra (Figure 5). It shows strong asymmetric Balmer and He I emission that shows remarkable inverse P Cygni line profiles with redshifted absorption and blueshifted emission. Figure 8 shows the line profiles relative to the systemic velocity of the He II photospheric lines. Such observations are usually interpreted as the infall of matter (e.g., Hartmann et al. 2016), which appears to imply a reabsorption of decretion disk material. The freefall velocity at the stellar surface for our adopted stellar parameters (Section 3.1) is $\sim$800 km s^{-1}, which is consistent with the red edge of the absorption trough seen in Hδ and He I λ4471. The Balmer emission-line intensities do not follow the Balmer decrement and are almost uniform (Figures 6 and 8), indicating optically thick emission. This suggests that the infalling material is also likely dense and thus has high emissivity.

Although epochs D and E are taken only 14 and 11 days before epoch F, respectively, epochs D and E show most lines in absorption with no sign of these features. Similarly, epoch G is obtained only 73 days after epoch F and also shows primarily an absorption spectrum. Thus, this infall episode corresponds to a short-lived event, which we fortuitously captured with this MIKE observation. In the spectra observed before and after epoch F, the Balmer emission, which presumably originates from the disk, does not seem substantially different in intensity. This suggests that the reabsorbed material corresponds to a negligible fraction of the disk mass. The timing of epoch F is at a very early phase, 0.024 (0.05), only 27 days after the light-curve minimum on MJD 57,626. There is no significant feature in the photometry near the time of epoch F, and the light curve is gradually brightening during this phase. This similarly implies that the continuum luminosity is dominated by the star and/or disk sources unrelated to the P Cygni event.

4. Disk Ejection Scenario

The distinctive shape of the light curve seen in 2002–2004 and again in 2016–2018, showing a strong drop in brightness followed by a gradual increase (Figure 1), is seen in some other emission-line stars (Rivinius et al. 2013). We suggest that this may be due to the repeated ejection of an optically thick circumstellar decretion disk, perhaps related to interaction with a binary companion. The exact reproduction of this part of the light curve across two cycles, starting with a 1.2 mag drop in brightness, suggests a geometric extinction effect caused by an optically thick disk. This event's pattern in photometry and Hβ line profile is consistent with a disk ejection outburst similar to, e.g., HD 38708 (Labadie-Bartz et al. 2017).

Assuming that an optically thick disk is indeed expelled to generate the deep light-curve minima ($I \sim 14.85$) in 2002 and 2016, we can estimate the geometric obscuration by considering the maximum flux following these minima, which peaks around $I \sim 14.0$. The difference of 0.85 mag corresponds to a reduction in flux by a factor of $\sim$0.46, or over half, assuming that all of this difference is due to obscuration. This suggests not only a fairly high angle of inclination but also a thick or, in particular, geometrically flared disk, which is consistent with the spectroscopic evidence (Section 3.3).

In this model, most of the emission lines originate from an inner disk region that experiences variable obscuration to our line of sight from a thicker outer disk or torus. The weaker spectroscopic epochs in Figure 5 with the typical OBe spectrum are the most obscured, while epochs A, B, and K are less obscured and therefore show stronger emission-line spectra. Epoch C is observed in 2016 at a phase of 0.01 (0.01) and thus near the same phase as the light-curve peak in late 2001 (2009; Figure 1, Table 1). However, as noted above (Section 2.1), although the light curve repeats the disk ejection pattern, there is no evidence of a corresponding peak preceding this sequence on the same timescale as that in 2002. The epoch C Hβ profile (Figure 7) is consistent with the optically thick disk already having formed. Epochs D and E, observed immediately after this minimum, are similarly unremarkable, although they cover a much shorter spectral range. Since we see that a putative disk ejection apparently occurred in 2016, it may be that the system has precessed such that an associated photometric outburst is obscured by the ejection process.

The emission lines in epoch A are dominated by higher-temperature species at larger radii, whereas epoch K shows the opposite effect (Section 3.3). Epoch A is consistent with very dense, optically thick disks that have extended vertical flaring, as shown in models by, e.g., Sigut et al. (2009), where the emission, including that from harder radiation, is dominated by this outer region. In contrast, the disk geometry at epoch K is dominated by high-density gas near the center and no flaring, thus differing significantly from epoch A. Epoch A is observed at a phase of 0.54 (0.08), and epoch K shows the system at a phase of 0.37 (0.74; Table 1, Figure 1). This suggests that the disk changes between having a large, flared outer region at epoch A that contributes significantly to the emission and a configuration where flaring is insignificant and emission is dominated by a dense central region at epoch K, perhaps also reaccreting material onto the star. The existence of two different components dominated by inner and outer regions, respectively, could also be due to disk tearing, resulting in an inner disk and outer expanding annulus with different inclinations (Marr et al. 2022; Suffak et al. 2022).

The decreasing Hβ peak separations seen from epoch C (346 km s^{-1}) to epochs J (303 km s^{-1}) and K (289 km s^{-1}; Table 1) suggest that the emission is weighted toward increasing radii over this period, which is consistent with the inner disk dissipating or forming an annular disk with an expanding inner radius. However, this scenario does not explain the strong line emission in epochs A and K (Figure 5), which have the minimum Hβ peak separations. If the inner radius is indeed expanding, then either the emitting region must become dense or the disk must precess to lower inclination angles to reveal stronger line emission. The latter could also contribute to a model in which the decreasing peak separation is due to decreasing obscuration of the disk, allowing emission at larger

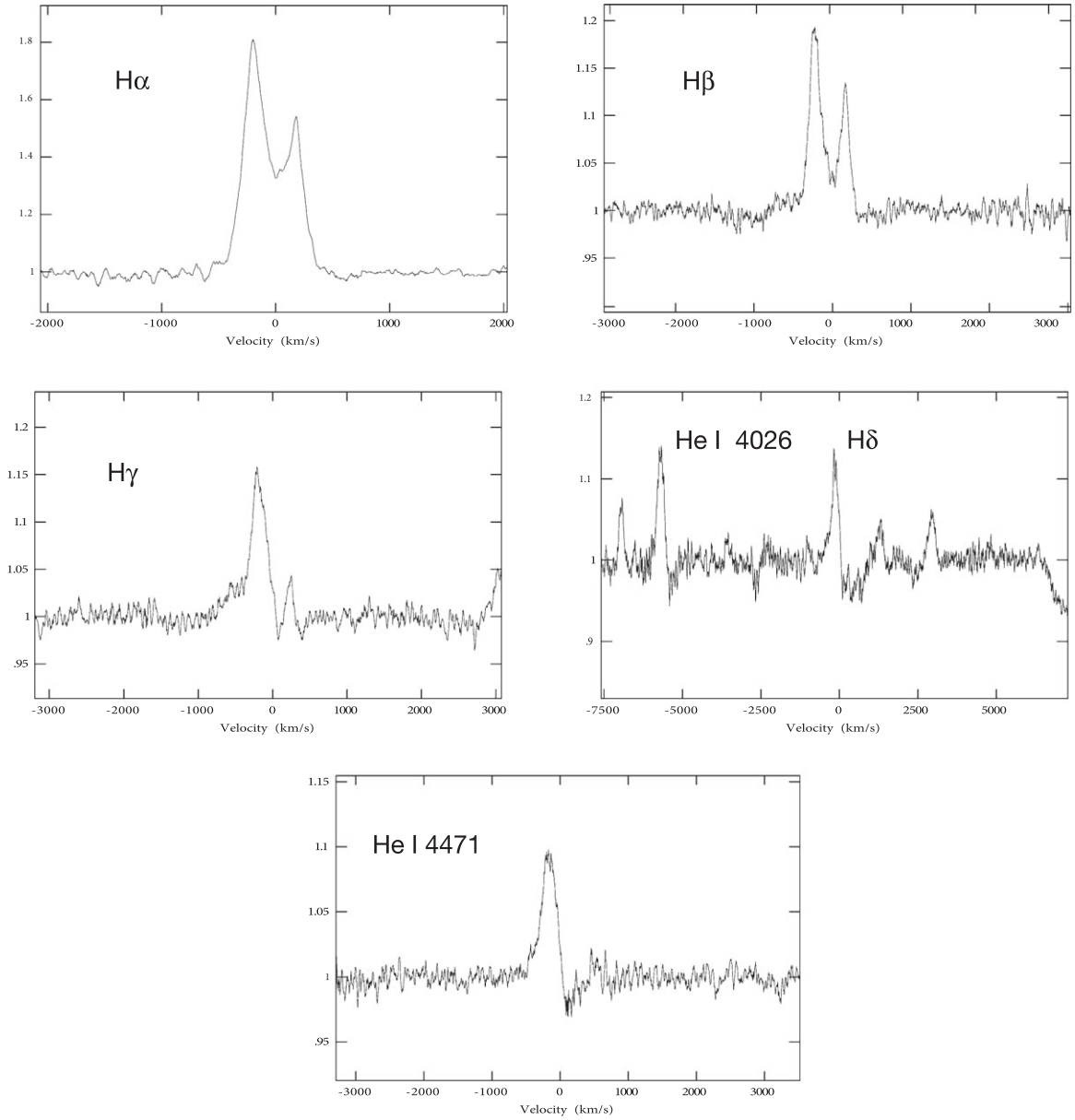

Figure 8. Epoch F line profiles for Balmer and He I emission lines, as shown, centered at the systemic velocity obtained from the He II absorption. This Magellan/MIKE observation was obtained on 2016 September 22 (Table 1).

radii to dominate. This is consistent with the system's increasing brightness over this period (Figure 1). The extinction may result from the outer component or optically thick torus or flare in the disk that either precesses or dissipates. However, we caution that such a fast precession rate may not be feasible. Moreover, if the long-term photometric cycle is due to precession, the light curve should be symmetric around the minima, whereas the observed strong, sudden drops (Figure 1) are difficult to explain with such a model.

The outflow and inflow episodes described in Section 3.4 apparently are not significant in mass relative to the entire disk. If the minima of the 14 yr light curve indeed correspond to the bulk of disk ejection, followed by gradual disk dissipation, then the mass ejection associated with the P Cygni features in epoch B are not likely to be a dominant source of disk material. However, we note that pulsations have been suggested to be important in replenishing the disk in other OBe systems (e.g., Baade et al. 2016, 2018).

The timing of epoch F is 27 days after the light-curve minimum on MJD 57,626. Although there are three other intermediate spectroscopic epochs between the putative disk ejection and epoch F, this still takes place during what we assume is the heavily obscured phase in the light curve. The lack of any photometric event near the appearance of inverse P Cygni features in epoch F suggests that the reabsorbed material is an insignificant portion of the disk material. The disk is therefore substantial and can plausibly provide material that may fall back to the star. This is consistent with the optically thick conditions indicated by the Balmer decrement in epoch F.

Thus, this model is driven by repeated ejection of a flared, optically thick disk whose outer region gradually dissipates, revealing the inner line-emitting region. A flared disk is most clearly implied by the ionization and emission-line peak separation in epoch A (Section 3.3) and is also consistent with a maximum geometric obscuration that may be >50% implied by this model. The spectroscopic variation could also be caused

by disk tearing or precession of the system. The decreasing trend in Hβ peak separations with increasing flux suggests that more light from larger radii can be seen (Section 3.2). Additionally, the high-amplitude, semiregular pulsations with the ∼month-long period become visible at low extinction (Figure 1). Other photometric and spectral variations may be due to contributions from the inner disk's radial expansion, reabsorption, or evaporation/ionization and possible geometric distortion or warping of the disk system.

5. Disk Growth Scenario

However, some observations seem inconsistent with a disk ejection model. For example, the system is bluest when faintest (Figure 1), contrary to expectations for reddening. As noted above, the strong emission-line spectra at epochs A and K seem inconsistent with the dissipating inner disk scenario implied by the trend in ΔHβ. If the long-period cycle is attributed to disk precession, it would require an additional mechanism to explain the asymmetric light curve, as well as a third, external massive star that is not seen, to torque the disk. Thus, alternative models for the AzV 493 system should also be considered.

Some other Be stars, such as δ Sco (Suffak et al. 2020) and ω CMa (Ghoreyshi et al. 2018), show long-term photometric variability in which the increasing flux is due to contributions from a growing disk, while the minima represent episodes of disk destruction by the secondary at periastron. Such a model is therefore opposite to the one presented above. In this alternative scenario, the light-curve minima of AzV 493 in 2002 and 2016 (Figure 1) correspond to episodes with the lowest disk contribution. The disk then grows and brightens, recovering its full size around 2005. In this case, the decreasing trend in Hβ peak separation with increasing flux is simply due to the disk growth itself. This scenario is consistent with the blue color at the light-curve minimum in 2016 (Figure 1) and the weak emission-line spectra near the 2016 minimum (epochs C–J; Figure 5).

If the disk is responsible for the factor of 2.2 increase in flux, then the equivalent width (EW) of the stellar absorption features should decrease proportionately. Figure 9 shows the EW of He II λ4200 and λ4540 as a function of V and I magnitude. A slight trend is indeed apparent, although not as large as a factor of 2 in amplitude. These lines are in the B band and thus not in the range of our photometry. Figure 1 shows that the amplitude of the photometric variations may be smaller at bluer wavelengths, although with the given V-band sampling, it is not entirely clear. It may be challenging for the alternative model to produce and maintain the viscous disk necessary to generate continuum luminosities that compete with those of the star, given the harsh circumstellar environment of an extreme early-type O star.

The extinction-dominated model is supported by the lack of correlation between the strength of the emission-line spectrum and photometric flux from the system. There is no significant variation between spectral epochs C–J (Figure 5), which should correspond to the period of strong disk growth in this model, whereas the obscuration-dominated model implies dissipation (Section 3.3). The one exception showing spectral variation, epoch F, has P Cygni emission and stronger emission-line features, yet it is photometrically unremarkable (Section 3.4). Another issue is that the photometric minimum corresponds to the bluest color (Figure 1), which is more consistent with the alternative model. However, the star itself may be changing substantially in magnitude and color. Blueing is also caused by scattering in high-extinction conditions, as seen in the UXOR class of Herbig Ae stars (Natta & Whitney 2000).

The overall shape of the light curve for AzV 493 is rather different from those of δ Sco and ω CMa, which show extended minima with more top hat–like light curves (Ghoreyshi et al. (2018; Suffak et al. 2020). In contrast, AzV 493 shows sharp minima (Figure 1), implying very rapid disk destruction and immediate, regular regrowth in the alternative model. It seems hard to explain such a sudden dissipation of a several-au dense, viscous disk by a neutron star or black hole (Section 6) during the brief periastron passage. Moreover, the exact reproduction of the photometric cycle's initial segment (Section 2.1) is unusual and may be harder to explain with a disk growth model.

Overall, the fundamental nature of the light curve and disk evolution remain unclear. Tailored modeling of this system and further multimode observational monitoring are needed to clarify the relationship between the decretion disk and interaction with a secondary star.

6. An Extreme Interacting Binary

The fast surface rotation for this evolved O star is a natural signature of accretion during a mass transfer event (e.g., Packet 1981; Cantiello et al. 2007; Renzo & Götberg 2021), consistent with an interacting binary scenario. If the disk is induced by a periastron passage of an undetected companion, then this may imply a long, 14.6 (7.3) yr period, and hence a large and highly eccentric orbit. For the AzV 493 stellar parameters obtained in Section 3.1, a neutron star companion of mass 1.4 $M_\odot$ would require $e \sim 0.95$ (0.93) and an apastron of ∼43 (27) au for a typical OBe star periastron distance of 40 $R_\star$. These orbital parameters are similar to those of the Be star δ Sco (e.g., Che et al. 2012). The unseen companion could also be a somewhat more massive main-sequence or stripped star or a black hole. The eccentricity may be lower, but if a binary companion is responsible for disk ejection, then periastron must be small and the eccentricity high. The nominal periastron value used here would likely be an upper limit, since δ Sco showed no disk ejection at periastron (Che et al. 2012).

6.1. Neutron Star or Black Hole?

Thus, if a binary companion excites disk ejection or is otherwise responsible for the observed properties of AzV 493, it is probably an eccentric system, and the most likely explanation for such an orbit is that the companion has already experienced core collapse, receiving a strong kick. Large natal kicks are routinely invoked in core-collapse events that form neutron stars (e.g., Arzoumanian et al. 2002; Podsiadlowski et al. 2004; Janka 2017; Verbunt et al. 2017). Natal kicks during black hole formation are still highly debated (e.g., Dray et al. 2005; Janka 2013; Mandel 2016; Repetto et al. 2017; Atri et al. 2019; Renzo et al. 2019; Callister et al. 2021) but not excluded. Assuming a large 450 km s^{-1} kick, Brandt & Podsiadlowski (1995) found a broad correlation between eccentricity and the orbital period of binaries surviving the first core collapse. This is in agreement with the high e and long period we find for AzV 493.

The present-day mass of AzV 493 can be used to constrain the nature of a putative compact object. Assuming a flat

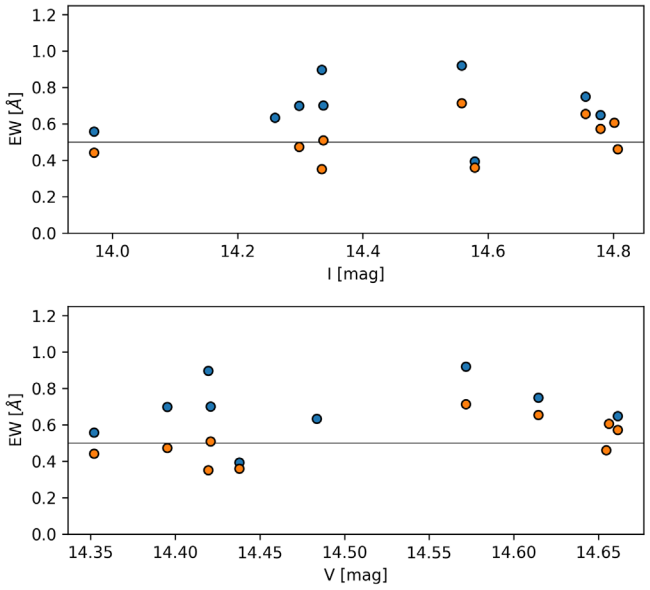

Figure 9. The EW of He II λ4200 (red) and λ4540 (blue) as a function of V (bottom) and I (top) magnitude. A constant value of 0.5 Å is shown for reference.

distribution in initial mass ratio, the average initial binary mass ratio $q = M_2/M_1 \simeq 0.5$ (e.g., Moe & Di Stefano 2017). Without any accretion during mass transfer, the present-day mass of AzV 493, $M_2 \simeq 50\,M_\odot$, would suggest $M_1 \simeq 100\,M_\odot$, which at SMC metallicity implies that the compact object should be a black hole (e.g., Sukhbold et al. 2016; Couch et al. 2020; Zapartas et al. 2021). In this case, however, the rapid rotation of AzV 493 would need to be primordial.

Instead, it is more likely that mass transfer has occurred, in which case M_1 is likely to be quite different, depending on the mass transfer efficiency. A mass transfer phase during the donor's main sequence (Case A) is expected to be slower and more conservative, possibly causing significant mass growth of the accretor without extreme chemical pollution. This scenario has been invoked to explain the formation of low-mass compact objects in very young regions (Belczynski et al. 2008) and, in particular, the origin of very massive companions (van der Meij et al. 2021), such as we have for AzV 493. In this case, the zero-age main-sequence (ZAMS) mass of $M_1 \sim 30$–40 $M_\odot$ for the adopted q, also accounting for the final donor core mass. However, mass transfer is far more likely to occur after the donor main sequence (Case B) due to the star's expansion (e.g., van den Heuvel 1969). It then takes place rapidly, on the thermal or He core-burning nuclear timescale (Klencki et al. 2022), and system mass loss is far more likely, implying a higher ZAMS mass for M_1.

Although post-SN outcomes are stochastic, black hole production is expected to dominate for $Z_\odot$ progenitors with initial masses $\gtrsim$20 $M_\odot$. This nominal threshold ZAMS mass is expected to decrease for lower metallicity (e.g., Zhang et al. 2008; O'Connor & Ott 2011; Sukhbold et al. 2016), which in principle enhances the likelihood that the compact object should be a black hole. The high eccentricity in AzV 493 strongly suggests that an SN occurred. While this implies that the companion is more likely to be a neutron star, black holes can form from fallback if the SN is insufficient to unbind the ejecta, which is more likely to happen at low metallicity (e.g., Zhang et al. 2008). There are multiple mechanisms to produce core-collapse black holes, and if mass loss occurs, an SN and/or a kick to the system may result (e.g., Janka 2013). We note that $M_1 \sim 20$–40 $M_\odot$ is a range that has been extensively simulated and where explodability and fallback are uncertain (e.g., O'Connor & Ott 2011; Sukhbold et al. 2016; Janka 2013; Zhang et al. 2008). Establishing that a neutron star or black hole resulted from this ZAMS range with some kind of kick would provide an important empirical reference for theoretical models of the explosion and the binary interactions preceding it.

Follow-up observations at subsequent periastra could more firmly establish whether AzV 493 has a companion and whether it is a black hole as opposed to a neutron star. A 74.33 ks Chandra/HRC observation on 2012 February 12 (MJD 55,969) of a field including AzV 493 (ObsID 14054) shows no detection. Given the tiny orbital interval during which the two stars interact, no significant accretion onto the compact object is expected, explaining why the system is not a known HMXB. However, well-timed X-ray observations near periastron may be able to catch a brief flare event.

6.2. Radial Velocities

We also measure the RV for the obtained spectra to search for evidence of a companion. This is challenging, since AzV 493 is a luminous, fast-rotating, early-type O star with few photospheric features, several of which are often in emission. We carried out cross-correlations against the FASTWIND model spectra for the entire observed spectral range using the iSpec code (Blanco-Cuaresma et al. 2014), as well as determinations based on cross-correlations against PoWR model spectra (Hainich et al. 2019) for only the He II lines (λ4200, λ4540, and λ4686 lines), which are the only clean features appearing in all epochs. The latter are carried out with the Markov Chain Monte Carlo code of Becker et al. (2015), and since they yield better results, we adopt these RV measurements (Table 1).

We find that the mean systemic RV is 202 ± 9 km s^{-1}, weighted inversely by the errors. We caution that the quoted standard error on this value underestimates the uncertainty if there is true variation. Given the difficulty of these measurements, with median errors on individual epochs of 46 km s^{-1}, it is difficult to evaluate any variability (Figure 10). There is possible evidence for very short term RV variations; however, the data are ambiguous.

We compute RV models for a possible periastron suggested in Section 2.3 at MJD 57,523, which is near the second minimum in the light curve (Figure 1). For this 7.3 yr period, and the above, nominal periastron distance of 40 $R_\star$, the eccentricity $e \sim 0.93$ and apastron $\sim$28 au. For this scenario, Figure 10 demonstrates that the RV signature of a neutron star companion at periastron is very brief, on the order of 0.01 in orbital phase, and moreover, the observational uncertainties are larger than the expected amplitude. This is the case even for $e = 0.99$. Thus, our existing RV measurements do not strongly constrain whether MJD 57,523 corresponds to a periastron nor the existence and properties of a companion.

6.3. Proper Motion

A post-SN bound system can be expected to have been accelerated from its original rest frame. Relative to the blue stars from Massey (2002) within a 5′ radius, the Gaia EDR3 (Gaia Collaboration et al. 2021) residual proper motions of

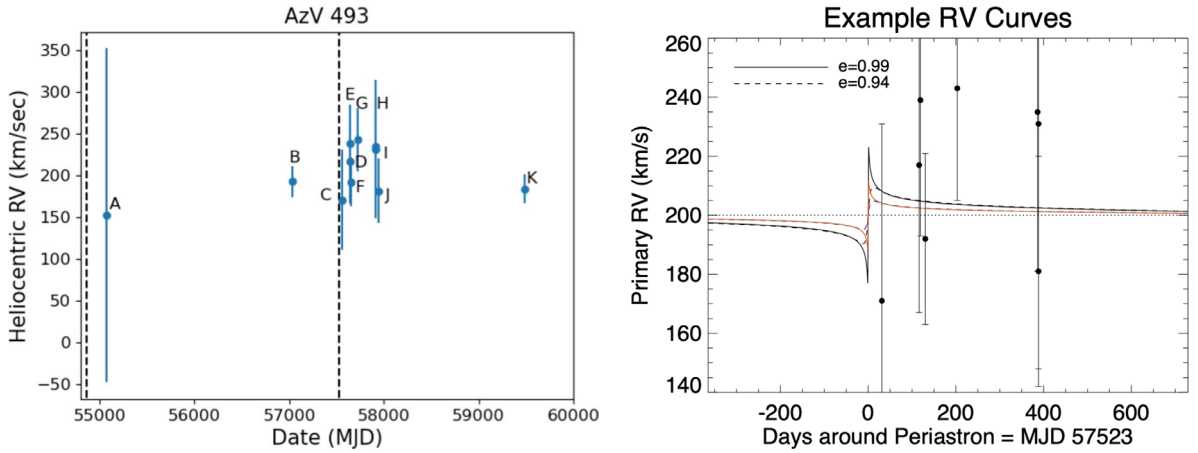

Figure 10. Left: heliocentric radial velocities measured from He II photospheric absorption vs. MJD for all epochs. Epoch A has only one available line of low quality and hence a very large uncertainty. The vertical dashed lines show the possible periastra at MJD 54,686 and 57,523. Right: zoom for the same data showing RV models for eccentricities of 0.94 (dashed lines) and 0.99 (solid lines), assuming a periastron occurs at MJD 57,523, and inclination angles of 90° (black) and 45° (blue) for the 50 $M_\odot$ primary and assuming a 3 $M_\odot$ secondary. If a periastron is closer to the light-curve minimum at MJD 57,626, the models would shift to 103 days later.

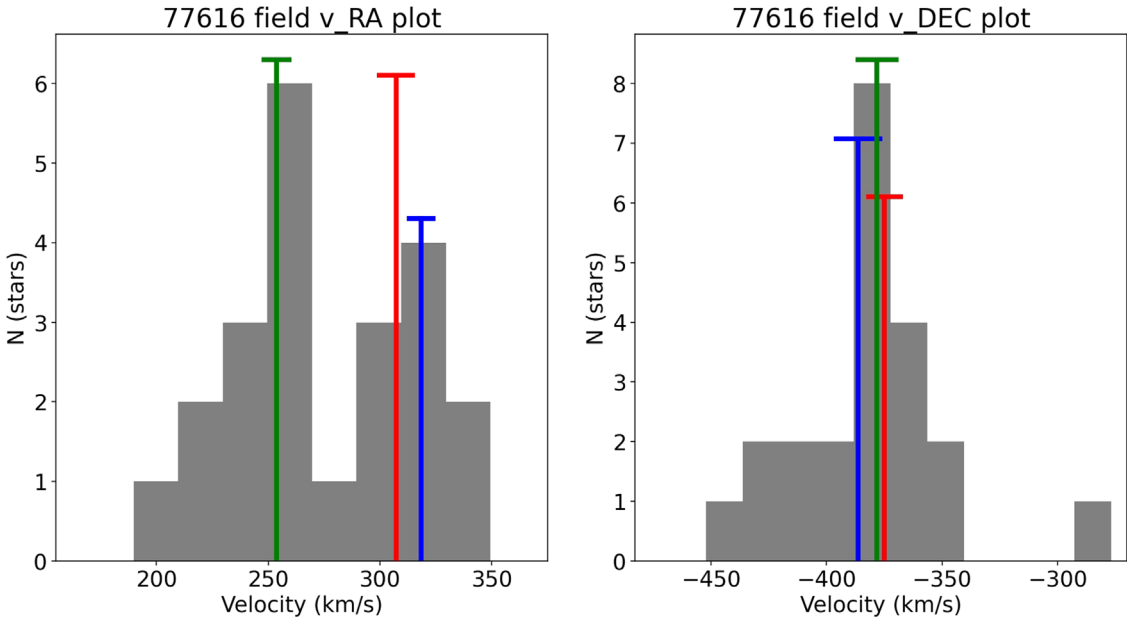

Figure 11. Distribution of Gaia proper-motion velocities in R.A. (left) and decl. (right) for stars from Massey (2002) within 5′ of AzV 493. The bimodal R.A. distribution defines two kinematic groups. The first group has 13 stars with median velocity $(v_\alpha, v_\delta) = (254 \pm 7, -378 \pm 9)$ km s^{-1}, and the second has 10 stars with $(v_\alpha, v_\delta) = (318 \pm 6, -386 \pm 11)$ km s^{-1}. The one star between the two groups in v_α is included in both. The median velocities for these groups are shown with the vertical green and blue lines, together with the velocity of AzV 493 (red).

AzV 493 show two potential velocity vectors. Figure 11 provides the velocity histograms of these local field stars, showing strong bimodality in the R.A. components. These define two possible local velocity fields, implying an R.A. and decl. residual velocity for AzV 493 of either $(v_\alpha, v_\delta) = (53 \pm 11, 3 \pm 12)$ or $(-11 \pm 11, 12 \pm 13)$ km s^{-1}. These yield total projected transverse velocities of 54 ± 11 or 16 ± 12 km s^{-1}.

Figure 12 shows a wide-field view of the surrounding environment with the two possible proper-motion vectors superposed. We see that the nearest massive star-forming region is the N84 complex (Henize 1956) about 15′–20′ or ∼300 pc to the west. If the velocity measurements are correct, the faster eastbound velocity is consistent with AzV 493 originating in N84 and traveling for $\gtrsim$5 Myr. The lifetime itself of a 50 $M_\odot$ star with $v \sin i \sim 500$ km s^{-1} is about 5 Myr (Brott et al. 2011), and for an SN ejection, its travel time would only be the post-SN lifetime. However, since the star presumably acquired its total mass and spin later in life, the system may have been ejected earlier by dynamical processes as a tight, non–compact binary. If so, it would have been reaccelerated by the SN explosion, therefore implying that it may be a two-step ejection (Pflamm-Altenburg & Kroupa 2010). The SN accelerations are typically weaker than dynamical ejections (e.g., Renzo et al. 2019), thus the dominant velocity component could still be due to a dynamical ejection from N84. A dynamically active past in a dense stellar environment of N84 may also help to explain the eccentricity (e.g., Simón-Díaz et al. 2015), although it would seem unlikely that the system could maintain its highly eccentric configuration for 5 Myr. On the other hand, we note that the inferred runaway velocity, orbital eccentricity, and period are still

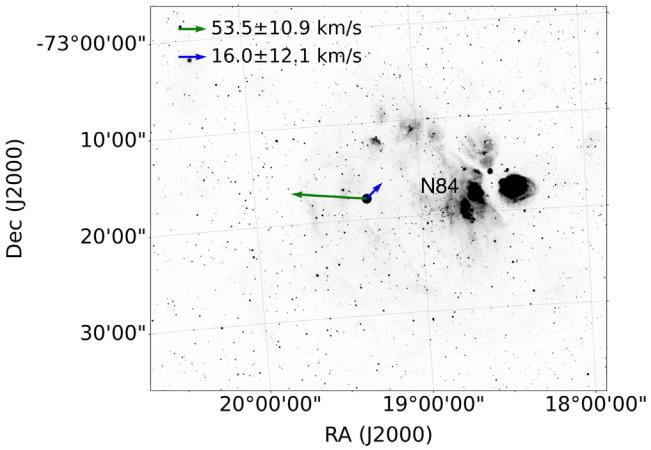

Figure 12. Location of AzV 493 in the SMC field, with the green and blue proper-motion vectors corresponding to the two field velocities indicated with the same color coding in Figure 11, superposed on an Hα image from Smith et al. (2005). The nearest massive star-forming region is the N84 complex (Henize 1956), which is indicated. For the adopted SMC distance, $10' = 181$ pc.

consistent with being due solely to SN acceleration (e.g., Brandt & Podsiadlowski 1995). Thus, in order to explain both the long travel time and high eccentricity, the most plausible scenario may be the two-step ejection.

There is also a small possibility that the slow, alternative proper-motion vector (Figure 12) is correct. However, this would mean that the AzV 493 system formed in isolation, since there is no corresponding young cluster whence it could have originated (Figure 11). Vargas-Salazar et al. (2020) found that <5% of OB stars, if any, formed in the field, and this is especially unlikely for AzV 493, given its high mass. We caution that the velocity errors do not include unknown systematic errors, thus these measurements need to be confirmed. Thus, although AzV 493 indeed appears to be a runaway star, this does not provide especially useful information to constrain its binary interaction history.

6.4. Similar Systems

A comprehensive study by Marr et al. (2022) shows that the B8 Vpe star Pleione (HD 23862) has a light curve with a similar long-term pattern of slow growth with sudden drops and similar variations in the Balmer emission-line profiles. It is a triple system with a close companion on a 218 day orbit (Katahira et al. 1996; Nemravová et al. 2010). Marr et al. (2022) suggested that the photometric drops correspond to the decretion disk tearing into two components, where one remains aligned with the star's equatorial plane and the other is misaligned due to tidal torque from the close companion. Pleione's long-term photometric cycle is 34 yr, similar in magnitude to that of AzV 493. Nemravová et al. (2010) found that the close companion is on an eccentric orbit with $e > 0.7$.

The initial peak brightness of AzV 493 and its subsequent drop in 2001 (Figure 1) qualitatively resemble the photometric pattern characteristic of heartbeat stars. These are a rare class of interacting binary systems with high eccentricities such that the periastron passage tidally induces regular photometric outbursts. However, the observed pattern in AzV 493 cannot be induced by this type of tidal interaction; preliminary simulations using new capabilities in the GYRE stellar oscillation code (Sun et al. 2023) suggest that the combined amplitude and width of the periastron pulse cannot be reproduced by eccentric tidal models. Nevertheless, given that AzV 493 seems likely to be a massive eccentric binary system, massive heartbeat stars thus share some similarities with this object if a companion indeed interacts with the primary and/or its disk. Examples include the non-Be binary system ι Ori (O9 III + B1 III/IV), which has an orbital period of 29 days and eccentricity $e = 0.764$, as determined by Pablo et al. (2017). They found that the two components have masses of 23.2 and 13.4 $M_\odot$, respectively, generating tidally excited oscillations with periods on the order of $\sim$1 day. MACHO 80.7443.1718 is another heartbeat system with two stars of type B0 Iae and O9.5 V and masses of 35 and 16 $M_\odot$, respectively (Jayasinghe et al. 2021).

The B0.5 Ve star δ Sco is has a B2 V star companion in an eccentric ($e = 0.94$) orbit with a period of 10.7 yr (e.g., Tango et al. 2009; Tycner et al. 2011). The two components have masses of 13.9 and 6 $M_\odot$ (Che et al. 2012). This system shows a long-term photometric cycle somewhat similar to that of AzV 493, although much more poorly defined. There is no obvious link between the disk properties and binary interaction (Che et al. 2012; Suffak et al. 2020), but the long-term photometry has a timescale similar to that of the orbital period.

Object H1145–619 is a Be X-ray binary whose primary is a B0.2e III star estimated to be 18.5 $M_\odot$ (Alfonso-Garzón et al. 2017), and the secondary is an X-ray pulsar. As shown by Alfonso-Garzón et al. (2017), H1145–619 has a light curve with an $\sim$10 yr cycle together with unexplained multiple modes of much shorter periods ($\sim$1 yr), qualitatively similar to what we see for AzV 493, which has a long cycle of 14.6 (7.3) yr and short oscillations of $\sim$40 days. While it remains unclear whether the light curves of H1145–619 and AzV 493 have fundamental similarities, both stars are massive OBe stars. If they are related, the fact that H1145–619 has a confirmed compact binary companion may suggest that the unusual variability of AzV 493 may have a similar origin.

These objects provide a context for AzV 493 that supports this object being a member of this broad class of binary, massive OBe systems with high eccentricities. At 50 $M_\odot$, AzV 493 is more massive than any of these similar objects. It is also one of the earliest O stars in the SMC, since there is no photospheric He I. Thus, AzV 493 may be the most extreme such object known in terms of its mass and effective temperature. Its variability amplitudes are also among the largest known.

We note that, based on only the epoch A spectrum (Figure 5), Golden-Marx et al. (2016) suggested that AzV 493 is a normal but extremely early classical Oe star. Given the strong spectroscopic and photometric variability, the nature of this spectrum may be somewhat different than inferred in that work, and the origin of the strong line emission seen in this particular spectrum is unclear (Section 3.3). Still, its status as a post-SN binary where the observed star was likely spun up by mass transfer from the compact object progenitor is consistent with the origin of classical OBe stars. Indeed, given that most of the massive OBe stars are post-SN systems (e.g., Dorigo Jones et al. 2020; Dallas et al. 2022), we can expect that more of them are likely to be high-eccentricity compact object binaries.

6.5. Alternative Companion Scenarios

We now consider alternative scenarios for a putative binary component. First, such a companion might be an unexploded

former donor in an interacting binary. In this case, it could be a stripped star (e.g., Götberg et al. 2017; Schootemeijer et al. 2018), which can be elusive to detect. Wang et al. (2021) identified hot, stripped star companions to Be stars based on far-UV spectral cross-correlations; however, the extremely hot temperature of AzV 493, which is commensurate with the hottest O stars, poses a serious challenge for this method. If the observed star has previously experienced accretion from binary mass transfer, then its surface might be He- and N-enriched (e.g., Blaauw 1993; Renzo & Götberg 2021), although whether this occurs depends on the accretion efficiency and mixing processes in the accretor's envelope. Since early O stars have few metal lines, it is again difficult to evaluate any enrichment, especially in a fast rotator like AzV 493. There is no immediate evidence for any unusual abundances in this star. Moreover, a nondegenerate companion does not naturally explain the high observed eccentricity, which would then have to be primordial, avoiding tidal dissipation, or of dynamical origin.

Alternatively, the high rotation rate and variability of AzV 493 might be caused by a nonstandard internal structure of the star because of a merger. These are common among massive stars, occurring in $22^{+26}_{-9}\%$ of isolated massive binaries (Renzo et al. 2019), with an even higher rate if accounting for the presence of further companions (e.g., Toonen et al. 2020). For example, η Car has been suggested to originate from a merger in a hierarchical triple system, resulting in a present-day eccentric binary (e.g., Hirai et al. 2021). However, η Car is a luminous blue variable star and has other substantial differences from AzV 493.

Yet another possibility is that AzV 493 might be a triple system with a third, also invisible, star on a shorter-period orbit. This speculative scenario might help to explain how the strong, 40 day pulsations are maintained (Section 2.2). It also might help explain the apparently sporadic ejection and accretion events seen in epochs B and F (Section 3.4). Such a system would be unstable, but the brief interaction phase with the secondary may enhance its longevity. We note that the system is unlikely to be a triple in which the third star has an even larger orbit than the secondary. Although high orbital eccentricities can be produced by Kozai–Lidov cycles in such a system, this high-eccentricity phase of the cycle is short in duration. Thus, such extreme eccentricity may require a triple or higher-order multiple-star interaction in the system's birth cluster and may be linked to a dynamical ejection of AzV 493 into the field. Overall, however, it is challenging to explain AzV 493 in terms of a triple-star scenario. Unfortunately, RV monitoring is complicated due to the technical difficulty and possible presence of varying stellar pulsations, so it will be hard to evaluate whether the system consists of more than two stars.

7. Summary

We present 18 yr of OGLE project photometric data and spectroscopic data over 12 yr revealing the remarkable variability of AzV 493. This is perhaps the earliest known classical Oe star, with $T_{\rm eff} = 42{,}000$ K, $\log L/L_{\odot} = 5.83 \pm 0.15$, and $R_{\star}/R_{\odot} = 15 \pm 3$. These parameters imply a mass of $50 \pm 9\ M_{\odot}$. The dominant photometric pattern is reproduced after 14.6 yr. There are also large, semiregular ~40 day pulsations of unknown origin, as well as other structure in the light curve. It is not a known HMXB. The observed $v\ \sin\ i = 370 \pm 40$ km s^{-1}, with a high inferred $\sin i$, suggesting a rotational velocity of 400−450 km s^{-1}. The system is ~300 pc from the nearest massive star-forming complex, and its proper motion shows that it is likely a runaway star from that region with a transverse velocity of 54 ± 11 km s^{-1} possibly having experienced two-step acceleration.

Altogether, the data suggest that this object is likely an eccentric, interacting binary system with an undetected compact companion. If so, the orbital period could correspond to the 14.6 (7.3) yr period, implying a high eccentricity of at least $e \sim 0.95$ (0.93) and an apastron of ~43 (28) au. If this binary scenario is correct, AzV 493 would be among the most extreme systems known in terms of its early spectral type, high mass, and extreme eccentricity.

In our favored model, an optically thick decretion disk is regularly ejected, likely by a periastron encounter. A two-component disk system forms, with the outer region responsible for the 0.85 mag drop in *I*-band flux, while the inner disk is the origin of most of the observed emission-line spectrum. The spectra appear to show varying relative contributions from the inner and outer regions, consistent with the optically thick outer region dissipating over the cycle. The outer region may correspond to a flared disk, torus, or possibly a separate inclined annulus formed by tearing from the inner disk. We see direct spectroscopic evidence for episodes of both matter ejection and infalling reabsorption of dense disk material onto the star. The lack of exact regularity of the photometric and spectroscopic variations in the cycle implies that the geometry and/or mechanics of the disk ejection may vary. An alternative, opposite model seen in some Be stars, in which the brightness increases due to contributions from growing disk emission (e.g., Ghoreyshi et al. 2018; Suffak et al. 2020), should also be considered.

If AzV 493 indeed has a highly eccentric orbit, it would suggest that the system experienced a strong SN kick, implying that the unseen companion is a neutron star or black hole. The high $v\ \sin\ i$ also suggests that mass transfer occurred before this event. For a conservative Case A mass transfer, the progenitor donor's ZAMS mass would be 30−40 $M_{\odot}$ for a typical $q \sim 0.5$, and it would be larger for nonconservative Case B mass transfer. This mass range is well within that suggested by models to produce black holes, although the occurrence of strong natal kicks in cases of black hole formation is less clear. Alternatively, the donor could be a stripped star; however, this scenario cannot explain the extreme eccentricity, which would have to be dynamical or primordial. The system could also be a merger, but the eruptions and long-term pulsations seem less consistent with this scenario. AzV 493 could possibly be a triple system, which might explain how the strong photometric oscillations are maintained (Section 6.5).

Establishing the existence and nature of the unseen companion(s) can provide important constraints on binary evolution, core explodability, and origin of compact binaries. AzV 493 may offer an opportunity to directly observe the relationship between the binary companion's dynamical interaction and the disk ejection. Since many classical OBe stars are massive post-SN objects, it suggests a likely link between OBe stars and massive eccentric systems. Further study of this fascinating object can more definitively confirm its status and exploit the opportunities it offers to learn about massive binary evolution and disk ejection.

We benefited from useful discussions with many people, including Jon Bjorkman, Paul Crowther, Julian Deman, Jim Fuller, Jay Gallagher, Carol Jones, Max Moe, Megan Reiter, Steve Shore, and Drew Weisserman. Many thanks to Juliette Becker for the use of her code and to Traci Johnson, Mario Mateo, and the M2FS Team for help with observing runs. We also thank the anonymous referees for valuable comments that greatly improved this paper. This work was supported by NSF grant AST-1514838 to M.S.O. and by the University of Michigan. N. Castro acknowledges funding from the Deutsche Forschungsgemeinschaft (DFG), CA 2551/1-1; M.R. is supported by EUH2020 OPTICON RadioNet Pilot grant No. 101004719; and R.H.D.T. is supported by NASA grant 80NSSC20K0515. This research made use of Astropy, a community-developed core Python package for astronomy (Astropy Collaboration et al. 2013). M.S.O. acknowledges MDRS, LLC, for pandemic hospitality.

Facilities: Magellan, OGLE, Gaia.

Appendix
Generalized Lomb–Scargle Periodograms

Figure 13 shows the individual generalized Lomb–Scargle periodograms (Zechmeister & Kürster 2009) and ancillary information for the six roughly contiguous OGLE data sets during ∼2010–2016 (Section 2.2).

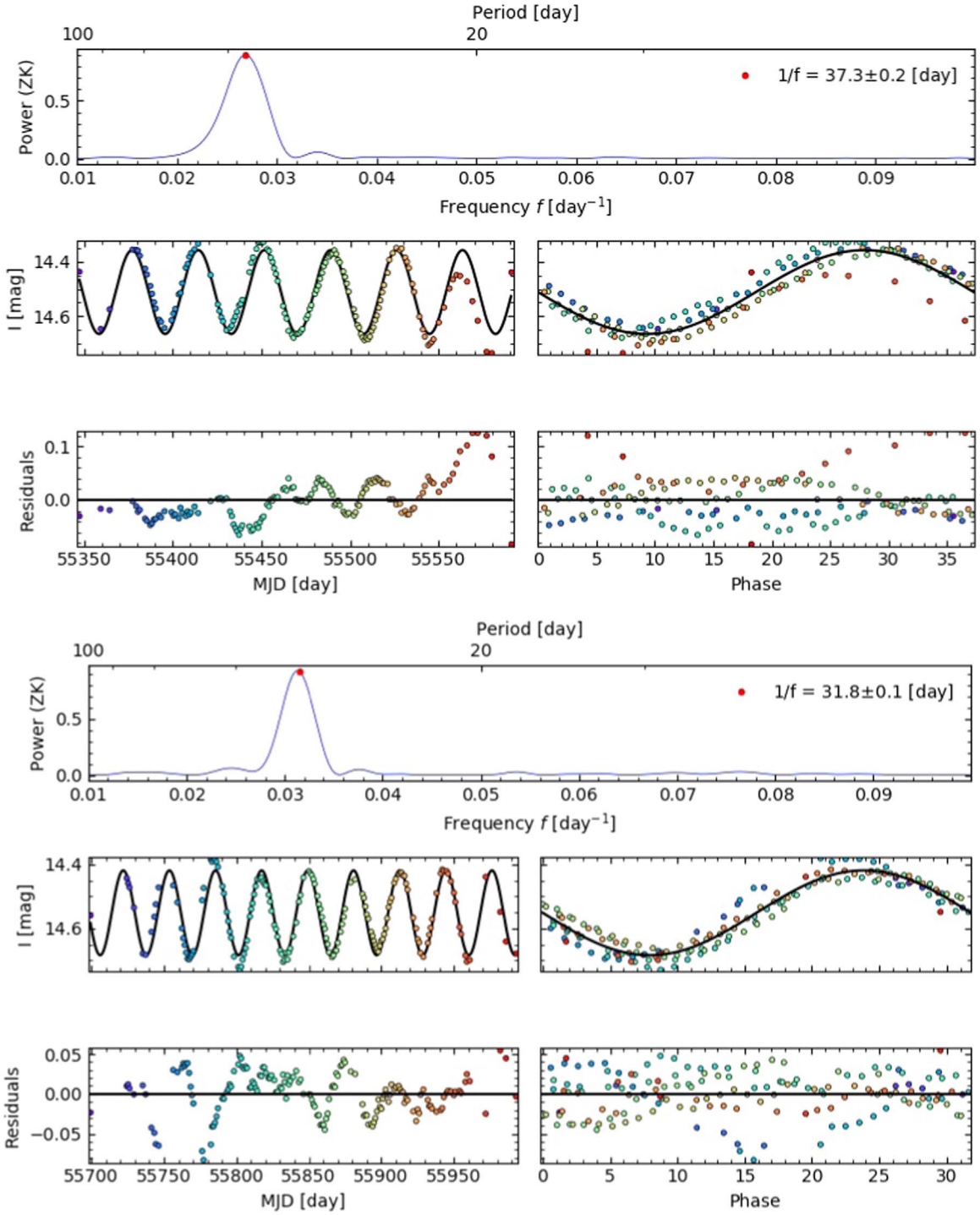

Figure 13. The top panels show the generalized Lomb–Scargle periodogram for light curves shown in the middle left panels. The fitted light curves are shown in the middle right panels, with each cycle superposed according to color from the middle left panel. Residuals are shown in the bottom panels as a function of MJD and phase. The middle and bottom panels have the same *x*-axes. The fitted period is shown in the top panel as the inverse of the frequency *f*. The observation time of spectroscopic epoch B is shown by the vertical dashed line in the plots for the fifth data set.

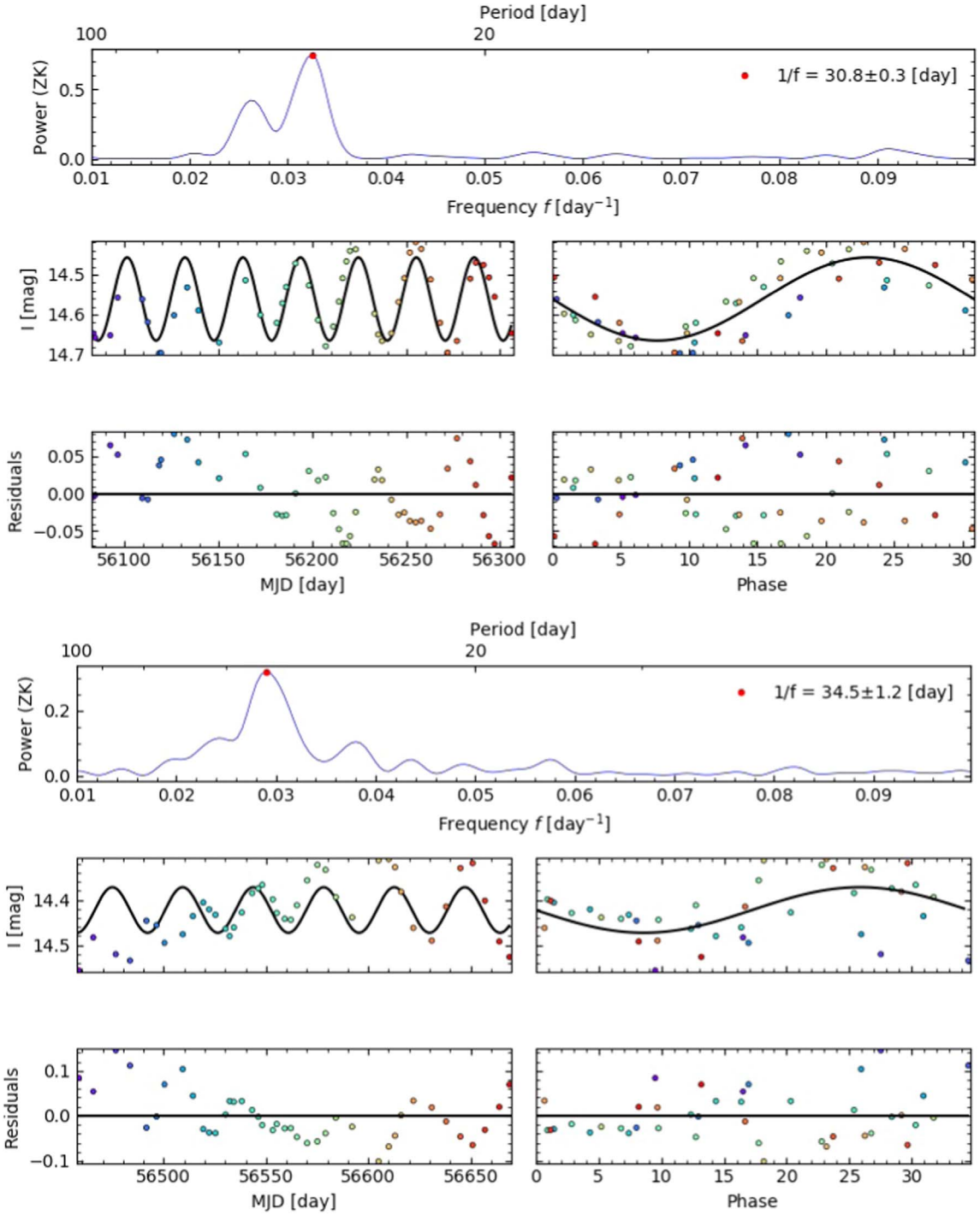

Figure 13. (Continued.)

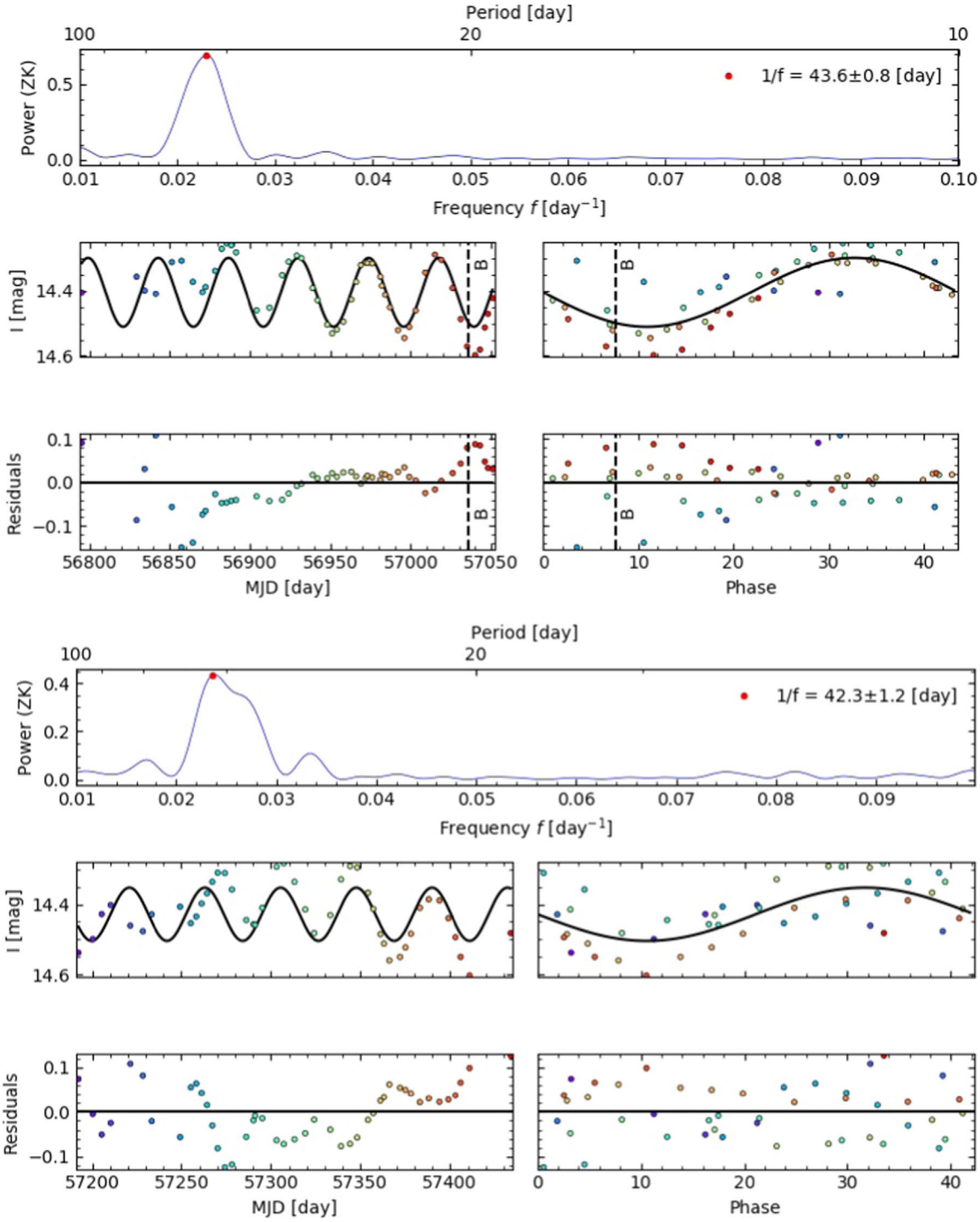

Figure 13. (Continued.)

ORCID iDs

M. S. Oey https://orcid.org/0000-0002-5808-1320
N. Castro https://orcid.org/0000-0003-0521-473X
M. Renzo https://orcid.org/0000-0002-6718-9472
I. Vargas-Salazar https://orcid.org/0000-0001-7046-6517
M. W. Suffak https://orcid.org/0000-0003-0696-2983
M. Ratajczak https://orcid.org/0000-0002-3218-2684
J. D. Monnier https://orcid.org/0000-0002-3380-3307
M. K. Szymanski https://orcid.org/0000-0002-0548-8995
G. D. Phillips https://orcid.org/0000-0002-8086-5906
N. Calvet https://orcid.org/0000-0002-3950-5386
A. Chiti https://orcid.org/0000-0002-7155-679X
G. Micheva https://orcid.org/0000-0003-4376-2841
K. C. Rasmussen https://orcid.org/0000-0002-0470-0800
R. H. D. Townsend https://orcid.org/0000-0002-2522-8605

References

Alfonso-Garzón, J., Fabregat, J., Reig, P., et al. 2017, A&A, 607, A52
Arzoumanian, Z., Chernoff, D. F., & Cordes, J. M. 2002, ApJ, 568, 289
Astropy Collaboration, Robitaille, T. P., & Tollerud, E. J. 2013, A&A, 558, A33

Atri, P., Miller-Jones, J. C. A., Bahramian, A., et al. 2019, MNRAS, 489, 3116
Azzopardi, M., Vigneau, J., & Macquet, M. 1975, A&AS, 22, 285
Baade, D., Pigulski, A., Rivinius, T., et al. 2018, A&A, 610, A70
Baade, D., Rivinius, T., Pigulski, A., et al. 2016, A&A, 588, A56
Becker, J. C., Johnson, J. A., Vanderburg, A., & Morton, T. D. 2015, ApJS, 217, 29
Belczynski, K., Kalogera, V., Rasio, F. A., et al. 2008, ApJS, 174, 223
Bernstein, R., Shectman, S. A., Gunnels, S. M., Mochnacki, S., & Athey, A. E. 2003, Proc. SPIE, 4841, 1694
Bigelow, B. C., & Dressler, A. M. 2003, Proc. SPIE, 4841, 1727
Blaauw, A. 1993, in ASP Conf. Ser. 35, Massive Stars: Their Lives in the Interstellar Medium, ed. J. Cassinelli & E. Churchwell (San Francisco, CA: ASP), 207
Blanco-Cuaresma, S., Soubiran, C., Heiter, U., & Jofré, P. 2014, A&A, 569, A111
Bodensteiner, J., Shenar, T., & Sana, H. 2020, A&A, 641, A42
Bonanos, A. Z., Lennon, D. J., Köhlinger, F., et al. 2010, AJ, 140, 416
Brandt, N., & Podsiadlowski, P. 1995, MNRAS, 274, 461
Brott, I., de Mink, S. E., Cantiello, M., et al. 2011, A&A, 530, A115
Callister, T. A., Farr, W. M., & Renzo, M. 2021, ApJ, 920, 157
Cantiello, M., Yoon, S., Langer, N., & Livio, M. 2007, A&A, 465, L29
Castro, N., Oey, M. S., Fossati, L., & Langer, N. 2018, ApJ, 868, 57
Che, X., Monnier, J. D., Tycner, C., et al. 2012, ApJ, 757, 29
Conti, P. S., & Leep, E. M. 1974, ApJ, 193, 113
Couch, S. M., Warren, M. L., & O'Connor, E. P. 2020, ApJ, 890, 127
Dallas, M. M., Oey, M. S., & Castro, N. 2022, ApJ, 936, 112
de Wit, W. J., Lamers, H. J. G. L. M., Marquette, J. B., & Beaulieu, J. P. 2006, A&A, 456, 1027
Dorigo Jones, J., Oey, M. S., Paggeot, K., Castro, N., & Moe, M. 2020, ApJ, 903, 43
Dray, L. M., Dale, J. E., Beer, M. E., Napiwotzki, R., & King, A. R. 2005, MNRAS, 364, 59
Fitzpatrick, E. L., & Massa, D. 2007, ApJ, 663, 320
Gaia Collaboration, Brown, A. G. A., Vallenari, A, et al. 2021, A&A, 649, A1
Ghoreyshi, M. R., Carciofi, A. C., Rímulo, L. R., et al. 2018, MNRAS, 479, 2214
Golden-Marx, J. B., Oey, M. S., Lamb, J. B., Graus, A. S., & White, A. S. 2016, ApJ, 819, 55
Götberg, Y., de Mink, S. E., & Groh, J. H. 2017, A&A, 608, A11
Graczyk, D., Pietrzyński, G., Thompson, I. B., et al. 2014, ApJ, 780, 59
Hainich, R., Ramachandran, V., Shenar, T., et al. 2019, A&A, 621, A85
Hartmann, L., Herczeg, G., & Calvet, N. 2016, ARA&A, 54, 135
Henize, K. G. 1956, ApJS, 2, 315
Hirai, R., Podsiadlowski, P., Owocki, S. P., Schneider, F. R. N., & Smith, N. 2021, MNRAS, 503, 4276
Janka, H.-T. 2013, MNRAS, 434, 1355
Janka, H.-T. 2017, ApJ, 837, 84
Jayasinghe, T., Kochanek, C. S., Strader, J., et al. 2021, MNRAS, 506, 4083
Katahira, J.-I., Hirata, R., Ito, M., et al. 1996, PASJ, 48, 317
Kelson, D. D. 2003, PASP, 115, 688
Kelson, D. D., Illingworth, G. D., van Dokkum, P. G., & Franx, M. 2000, ApJ, 531, 159
Klencki, J., Istrate, A., Nelemans, G., & Pols, O. 2022, A&A, 662, A56
Labadie-Bartz, J., Pepper, J., McSwain, M. V., et al. 2017, AJ, 153, 252
Lamb, J. B., Oey, M. S., Segura-Cox, D. M., et al. 2016, ApJ, 817, 113
Mandel, I. 2016, MNRAS, 456, 578
Marr, K. C., Jones, C. E., Tycner, C., Carciofi, A. C., & Silva, A. C. F. 2022, ApJ, 928, 145
Martins, F., & Palacios, A. 2021, A&A, 645, A67
Martins, F., Schaerer, D., & Hillier, D. J. 2005, A&A, 436, 1049
Massey, P. 2002, ApJS, 141, 81
Mateo, M., Bailey, J. I., Crane, J., et al. 2012, Proc. SPIE, 8446, 84464Y
Moe, M., & Di Stefano, R. 2017, ApJS, 230, 15
Natta, A., & Whitney, B. A. 2000, A&A, 364, 633
Nemravová, J., Harmanec, P., Kubát, J., et al. 2010, A&A, 516, A80
O'Connor, E., & Ott, C. D. 2011, ApJ, 730, 70
Okazaki, A. T. 1991, PASJ, 43, 75
Pablo, H., Richardson, N. D., Fuller, J., et al. 2017, MNRAS, 467, 2494
Packet, W. 1981, A&A, 102, 17
Pflamm-Altenburg, J., & Kroupa, P. 2010, MNRAS, 404, 1564
Podsiadlowski, P., Langer, N., Poelarends, A. J. T., et al. 2004, ApJ, 612, 1044
Poeckert, R. 1982, in IAU Symp. 98, Be Stars (Dordrecht: Reidel), 453
Poleski, R., Soszyński, I., Udalski, A., et al. 2012, AcA, 62, 1
Pols, O. R., Cote, J., Waters, L. B. F. M., & Heise, J. 1991, A&A, 241, 419
Puls, J., Urbaneja, M. A., Venero, R., et al. 2005, A&A, 435, 669
Renzo, M., & Götberg, Y. 2021, ApJ, 923, 277
Renzo, M., Zapartas, E., de Mink, S. E., et al. 2019, A&A, 624, A66
Repetto, S., Igoshev, A. P., & Nelemans, G. 2017, MNRAS, 467, 298
Richardson, N. D., Thizy, O., Bjorkman, J. E., et al. 2021, MNRAS, 508 2002
Rivero González, J. G., Puls, J., Massey, P., & Najarro, F. 2012, A&A, 543, A95
Rivinius, T., Carciofi, A. C., & Martayan, C. 2013, A&ARv, 21, 69
Santolaya-Rey, A. E., Puls, J., & Herrero, A. 1997, A&A, 323, 488
Schootemeijer, A., Götberg, Y., de Mink, S. E., Gies, D., & Zapartas, E. 2018, A&A, 615, A30
Sigut, T. A. A., McGill, M. A., & Jones, C. E. 2009, ApJ, 699, 1973
Simón-Díaz, S., & Herrero, A. 2007, A&A, 468, 1063
Simón-Díaz, S., & Herrero, A. 2014, A&A, 562, A135
Simón-Díaz, S., Caballero, J. A., Lorenzo, J., et al. 2015, ApJ, 799, 169
Skrutskie, M. F., Cutri, R. M., Stiening, R., et al. 2006, AJ, 131, 1163
Smith, R. C., Points, S. D., Chu, Y.-H., et al. 2005, AAS Meeting, 207, 25.07
Sota, A., Maíz Apellániz, J., Walborn, N. R., et al. 2011, ApJS, 193, 24
Suffak, M., Jones, C. E., & Carciofi, A. C. 2022, MNRAS, 509, 931
Suffak, M. W., Jones, C. E., Tycner, C., et al. 2020, ApJ, 890, 86
Sukhbold, T., Ertl, T., Woosley, S. E., Brown, J. M., & Janka, H.-T. 2016, ApJ, 821, 38
Sun, M., Townsend, R. H. D., & Guo, Z. 2023, ApJ, 945, 43
Tango, W. J., Davis, J., Jacob, A. P., et al. 2009, MNRAS, 396, 842
Tauris, T. M., & Takens, R. J. 1998, A&A, 330, 1047
Toonen, S., Portegies Zwart, S., Hamers, A. S., & Bandopadhyay, D. 2020, A&A, 640, A16
Tycner, C., Ames, A., Zavala, R. T., et al. 2011, ApJL, 729, L5
Udalski, A., Szymanski, M. K., Soszynski, I., & Poleski, R. 2008, AcA, 58, 69
Udalski, A., Szymański, M. K., & Szymański, G. 2015, AcA, 65, 1
van den Heuvel, E. P. J. 1969, AJ, 74, 1095
van der Meij, V., Guo, D., Kaper, L., & Renzo, M. 2021, A&A, 655, A31
Vargas-Salazar, I., Oey, M. S., Barnes, J. R., et al. 2020, ApJ, 903, 42
Verbunt, F., Igoshev, A., & Cator, E. 2017, A&A, 608, A57
Vinciguerra, S., Neijssel, C. J., Vigna-Gomez, A., et al. 2020, MNRAS, 498, 4705
Walker, M. G., Mateo, M., Olszewski, E. W., et al. 2015, ApJ, 808, 108
Wang, L., Gies, D. R., Peters, G. J., et al. 2021, AJ, 161, 248
Zapartas, E., Renzo, M., Fragos, T., et al. 2021, A&A, 656, L19
Zechmeister, M., & Kürster, M. 2009, A&A, 496, 577
Zhang, W., Woosley, S. E., & Heger, A. 2008, ApJ, 679, 639